



**HAL**  
open science

# An explicit well-balanced scheme on staggered grids for barotropic Euler equations

Thierry Goudon, Sebastian Minjeaud

► **To cite this version:**

Thierry Goudon, Sebastian Minjeaud. An explicit well-balanced scheme on staggered grids for barotropic Euler equations. *ESAIM: Mathematical Modelling and Numerical Analysis*, 2024, 58 (4), pp.1263-1299. 10.1051/m2an/2024035 . hal-04294768

**HAL Id: hal-04294768**

**<https://hal.science/hal-04294768v1>**

Submitted on 20 Nov 2023

**HAL** is a multi-disciplinary open access archive for the deposit and dissemination of scientific research documents, whether they are published or not. The documents may come from teaching and research institutions in France or abroad, or from public or private research centers.

L'archive ouverte pluridisciplinaire **HAL**, est destinée au dépôt et à la diffusion de documents scientifiques de niveau recherche, publiés ou non, émanant des établissements d'enseignement et de recherche français ou étrangers, des laboratoires publics ou privés.

# An explicit well-balanced scheme on staggered grids for barotropic Euler equations

Thierry Goudon\* and Sebastian Minjeaud†

Université Côte d’Azur, CNRS, Inria, LJAD  
Parc Valrose, F-06108 Nice, France

## Abstract

In this paper, we introduce a specific modification of the numerical fluxes in order to insure the well-balanced property of schemes on staggered grids for the Euler equations. This property is crucial for the numerical representation of equilibrium solutions of balance laws with source terms, like when describing flows subjected to gravity and a complex topography. We propose first and second order versions of the well-balanced scheme. The performances of the method are evaluated through a series of 1D and 2D benchmarks.

**MSC:** 65M08, 76M12, 76NXX, 35Q31.

**Keywords:** Finite volume schemes. Staggered grids. Well-balanced schemes. Balance laws. Shallow-water.

## Contents

<b>1</b>	<b>Introduction</b>	<b>2</b>
<b>2</b>	<b>Well-balanced scheme for the barotropic Euler system</b>	<b>3</b>
2.1	Staggered scheme: notation and definitions . . . . .	3
2.2	Incorporation of the source terms . . . . .	7
2.3	Second order version of the WB scheme . . . . .	12

---

\*thierry.goudon@inria.fr

†sebastian.minjeaud@unice.fr

<b>3</b>	<b>Numerical experiments</b>	<b>15</b>
3.1	Lake at rest . . . . .	15
3.2	Perturbations of the lake at rest solution . . . . .	16
3.3	Flow over an isolated bump . . . . .	16
3.3.1	Cases $F_0 = 0.2$ and $F_0 = 1.9$ . . . . .	21
3.3.2	Case $F_0 = 0.3$ . . . . .	23
3.3.3	Case $F_0 = 0.7$ . . . . .	23
3.4	Wet/dry fronts in a nonflat bassin . . . . .	26
3.5	Thacker test: oscillation in a 2D-paraboloid . . . . .	26

# 1 Introduction

The motivation of this paper comes from the development of numerical strategies to compute the solutions of complex flows, by working on staggered grids. This means that the numerical unknowns are stored in different locations, depending on their type. This is in contrast with the standard approach when dealing with systems of conservation laws, and a specific analysis should be developed for such schemes. It is expected that such an alternative approach might have some advantages when dealing with certain asymptotic regimes, like the low Mach regimes, or when some incompressibility-like constraint arises in the model, see for instance [11, 30, 39] and the references therein. Indeed, working with colocalized unknowns might lead to spurious instabilities, a difficulty that can be fixed by adopting dual discretizations, as illustrated by the MAC scheme for incompressible viscous flows [34]. In fact, schemes on staggered grids are widely used for CFD applications in industrial context, in particular for applications in defense, astrophysics, weather forecast or nuclear safety [1, 3, 4, 8, 58]. Most of these hydrocodes relies on the Lagrangian framework, in the spirit on the pioneering schemes introduced in [55, 59], see the recent analysis in [19, 44]. Our work is concerned instead with Eulerian methods, in the spirit of [4, 9, 10, 27, 26, 35, 37, 38, 42, 49, 52, 54, 56, 57]: Eulerian numerical methods on staggered grids have been developed and analyzed for the simulation of the Euler system, in the barotropic case as well as for the full set of equations, in one and multi-dimensions, including with second-order extensions [31, 27] or considering unstructured grids [32, 36].

Here, we address the issue of the treatment of *source terms* in such a staggered framework. Indeed, it is well-known that a direct discretization of the source terms, say for instance the gravity force, leads to inaccurate results, due to the inability to preserve steady state solutions. A classical illustration is the simulation of the Shallow Water system with topography. The difficulty has been pointed out on the seminal papers [2, 14, 33] which have given raise to many progress in order to design suitable methods that can handle accurately the source terms, for scalar equations [12], and for systems [6, 5, 7, 15, 43]; we refer the reader to the detailed presentations in [13, 29]. The basic idea behind most of these methods is to modify the numerical fluxes by a hydrostatic reconstruction and to introduce a source discretization to balance the flux difference, compatible with the equilibrium state.

The paper is organized as follows. Section 2 explains how the source terms can be incorporated in the staggered mass and momentum fluxes. We detail the consistency analysis, the well-balanced property and we identify the stability condition that guarantees the preservation of non negative densities. Next, we detail how the scheme can be modified in order to reach the second order accuracy, in the spirit of MUSCL procedures. Section 3 illustrates the abilities of the scheme in capturing equilibrium solutions, through a series of standard test cases in 1D and 2D.

## 2 Well-balanced scheme for the barotropic Euler system

### 2.1 Staggered scheme: notation and definitions

We consider the one-dimensional barotropic Euler system

$$\begin{cases} \partial_t \rho + \partial_x (\rho u) = 0, \\ \partial_t (\rho u) + \partial_x (\rho u \otimes u) + \partial_x (p(\rho)) = -\rho \partial_x z. \end{cases} \quad (1)$$

This model describes the evolution of a compressible fluid: the unknowns  $\rho$  and  $u$  stand respectively for the local density and velocity field of the fluid. They depend on the time and space variables,  $t \geq 0$  and  $x \in \mathbb{R}$ . The pressure  $p$  depends on the density  $\rho$  only: we suppose that  $\rho \mapsto p(\rho)$  belongs to  $C^1([0, \infty)) \cap C^2(]0, \infty))$  and satisfies  $p(0) = 0$ ,  $p'(0) = 0$  and

$$p(\rho) > 0, \quad p'(\rho) > 0, \quad p''(\rho) \geq 0, \quad \forall \rho > 0.$$

For instance, these properties hold for  $p(\rho) = \kappa \rho^\gamma$  with  $\kappa > 0$  and  $\gamma > 1$ . The force density function  $x \mapsto z(x)$  is given. We refer the reader to the classical treatises [18, 28, 46, 51] for a thorough introduction to these equations and for a description of the numerical issues. A case of particular interest is when  $\gamma = 2$  (and  $\kappa = 1/2$ ): the corresponding Shallow-Water system describes the free surface of a layer of fluid of constant density in hydrostatic balance, bounded from below by the bottom topography. In this case,  $\rho$  stands for the water depth, and  $z$  defines the bottom topography. In what follows, formula that apply to this specific case are distinguished by the tag **(SW)**.

As said above, preserving numerically the equilibrium solutions is far from obvious. Here, we focus on the equilibrium states *at rest* that satisfy

$$u = 0, \quad \partial_x p = -\rho \partial_x z.$$

Let us set

$$\mathcal{E}(\rho) = \frac{p(\rho)}{\rho} + \int_0^\rho \frac{p(s)}{s^2} ds$$

so that

$$\mathcal{E}'(\rho) = \frac{p'(\rho)}{\rho}.$$

Therefore, the equilibrium satisfy

$$\mathcal{E}(\rho) + z = \text{constant}.$$

In the specific case of the Shallow-Water system, we simply have

$$\text{(SW)} \quad p(\rho) = \frac{\rho^2}{2}, \quad \mathcal{E}(\rho) = \rho.$$

In the general case,  $\mathcal{E}$  is a strictly increasing function on  $[0, \infty[$  with  $\mathcal{E}(0) = 0$ . Thus, it is a one-to-one function from  $[0, \infty[$  to its range and we denote by  $\mathcal{E}^{-1}$  the inverse function of  $\mathcal{E}$ .

We address the issue of preserving equilibrium in the framework of staggered grids, with numerical densities and velocities stored in different locations. According to Fig. 1,

- we introduce a set of  $J + 1$  points  $x_1 = 0 < x_2 < \dots < x_J < x_{J+1} = L$  in the computational domain; we denote by  $\mathcal{C}_{j+\frac{1}{2}} = [x_j, x_{j+1}]$ ,  $j \in \llbracket 1, J \rrbracket$ , the cells defined by these points;
- we denote by  $x_{j+\frac{1}{2}} = (x_j + x_{j+1})/2$ ,  $j \in \llbracket 1, J \rrbracket$ , the centers of the cells; these points define the dual cells  $\mathcal{C}_j = [x_{j-\frac{1}{2}}, x_{j+\frac{1}{2}}]$ ,  $j \in \llbracket 2, J \rrbracket$ ;
- we set the following notation for the mesh-sizes

$$\delta x_{j+\frac{1}{2}} = x_{j+1} - x_j, \quad j \in \llbracket 1, J \rrbracket, \quad \text{and} \quad \delta x_j = \frac{\delta x_{j-\frac{1}{2}} + \delta x_{j+\frac{1}{2}}}{2}, \quad j \in \llbracket 2, J \rrbracket,$$

(with the specific definition for the end-cells:  $\delta x_1 = \frac{1}{2}\delta x_{\frac{3}{2}}$  and  $\delta x_{J+1} = \frac{1}{2}\delta x_{J+\frac{1}{2}}$ ). The discrete densities  $\rho_{j+\frac{1}{2}}$  are thought of as approximation of the density  $\rho$  on the cells  $\mathcal{C}_{j+\frac{1}{2}}$  whereas the discrete velocities  $u_j$  are thought of as approximation of the velocity  $u$  on the cells  $\mathcal{C}_j$ . Here and below, we denote

$$\delta x = \max \{ \delta x_j, \delta x_{j+\frac{1}{2}}, \quad j \in \{1, \dots, J\} \}.$$

Throughout the paper we shall use the notation

$$[z]_+ = \max(0, z) \geq 0, \quad [z]_- = \min(0, z) \leq 0.$$

In what follows, we denote  $(\hat{u}_j, \hat{\rho}_{j+\frac{1}{2}})$  a discrete equilibrium at rest with possibly a dry area, thus characterized by

$$\hat{u}_j = 0, \quad \mathcal{E}(\hat{\rho}_{j+\frac{1}{2}}) + z_{j+\frac{1}{2}} = \max(\eta, z_{j+\frac{1}{2}}). \quad (2)$$

where  $\eta \in \mathbb{R}$  is a given constant. We address the question of the conservation of such an equilibrium by the numerical scheme.

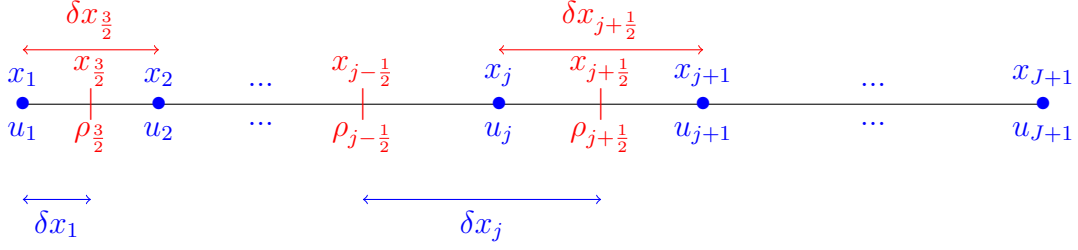


Figure 1: Staggered grid in dimension one.

With these notations, we update the numerical unknowns, having at hand the  $\rho_{j+1/2}$ 's and the  $u_j$ 's, by

$$\frac{\bar{\rho}_{j+1/2} - \rho_{j+1/2}}{\delta t} + \frac{\mathcal{F}_{j+1} - \mathcal{F}_j}{\delta x_{j+1/2}} = 0, \quad (3)$$

$$\frac{\bar{\rho}_j \bar{u}_j - \rho_j u_j}{\delta t} + \frac{\mathcal{G}_{j+1/2} - \mathcal{G}_{j-1/2}}{\delta x_j} + \frac{\Pi_{j+1/2} - \Pi_{j-1/2}}{\delta x_j} = -S_j, \quad (4)$$

where the overlined quantities  $\bar{\rho}_{j+1/2}$ ,  $\bar{\rho}_j \bar{u}_j$  denotes the updated numerical unknowns and  $\rho_j$  is an averaged quantity on the cell  $\mathcal{C}_j$  (see (9) below). These discrete formula are intended to mimic the integration of the mass conservation equation over  $[n\delta t, (n+1)\delta t] \times \mathcal{C}_{j+1/2}$  and of the momentum balance over  $[n\delta t, (n+1)\delta t] \times \mathcal{C}_j$ : the details of the numerical methods depend on the design of the numerical fluxes  $\mathcal{F}_j, \mathcal{G}_{j+1/2}, \Pi_{j+1/2}$  on the interfaces of the control volumes. The construction uses the values of the unknowns stored on the interface and in the neighbouring cells. Namely, our study is motivated by the scheme defined in [10, 11, 31]: taking into account the characteristic speeds of the system

$$\lambda_{\pm}(\rho, u) = u \pm c(\rho), \quad c(\rho) = \sqrt{p'(\rho)},$$

we adopt the following definition that relies on the upwinding principles,

$$\mathcal{F}_j = \mathcal{F}_j^+ + \mathcal{F}_j^-,$$

with

$$\mathcal{F}_j^+ = \mathcal{F}^+(\rho_{j-1/2}, u_j) \quad \text{and} \quad \mathcal{F}_j^- = \mathcal{F}^-(\rho_{j+1/2}, u_j). \quad (5)$$

The flux functions  $\mathcal{F}^{\pm}$  are given by

$$\mathcal{F}^+(\rho, u) = \begin{cases} 0 & \text{if } u \leq -c(\rho), \\ \frac{\rho}{4c(\rho)}(u + c(\rho))^2 & \text{if } |u| \leq c(\rho), \\ \rho u & \text{if } u \geq c(\rho), \end{cases} \quad (6)$$

and

$$\mathcal{F}^-(\rho, u) = \begin{cases} \rho u & \text{if } u \leq -c(\rho), \\ -\frac{\rho}{4c(\rho)}(u - c(\rho))^2 & \text{if } |u| \leq c(\rho), \\ 0 & \text{if } u \geq c(\rho). \end{cases} \quad (7)$$

This simple formula is inspired from the kinetic schemes [17, 22, 23, 41, 47, 48] since they can be defined through a “microscopic velocity variable”

$$\mathcal{F}^\pm(\rho, u) = \int_{\pm\xi > 0} M_{\rho, u}(\xi) d\xi,$$

where  $M_{\rho, u}$  is the “Maxwellian state”

$$M_{\rho, u}(\xi) = \frac{1}{2c(\rho)} \mathbf{1}_{|\xi - u| \leq c(\rho)}.$$

An alternative definition of the numerical fluxes can be obtained by using the Dirac mass centred on the material velocity:  $M_{\rho, u}(\xi) = \delta(\xi - u)$ ; this gives the scheme introduced in [37]. As a matter of fact, the flux function satisfy the symmetry property

$$\mathcal{F}^-(\rho, u) = -\mathcal{F}^+(\rho, -u),$$

and the flux-consistency condition

$$\mathcal{F}^+(\rho, u) + \mathcal{F}^-(\rho, u) = \rho u. \quad (8)$$

For stability analysis, it is important to observe that

$$\rho \mapsto \pm \mathcal{F}^\pm(\rho, u) \text{ are non decreasing functions.}$$

We turn to the momentum balance. We start by setting

$$\rho_j = \frac{\delta x_{j+\frac{1}{2}} \rho_{j+\frac{1}{2}} + \delta x_{j-\frac{1}{2}} \rho_{j-\frac{1}{2}}}{2\delta x_j}, \quad (9)$$

and

$$\mathcal{F}_{j+\frac{1}{2}}^\pm = \frac{\mathcal{F}_j^\pm + \mathcal{F}_{j+1}^\pm}{2}, \quad \mathcal{F}_{j+\frac{1}{2}} = \mathcal{F}_{j+\frac{1}{2}}^+ + \mathcal{F}_{j+\frac{1}{2}}^-. \quad (10)$$

Remarkably, the conservation relation

$$\bar{\rho}_j - \rho_j + \frac{\delta t}{\delta x_j} (\mathcal{F}_{j+\frac{1}{2}} - \mathcal{F}_{j-\frac{1}{2}}) = 0 \quad (11)$$

holds. The convection fluxes are obtained by applying the UpWinding principle, based on the “sign” of the mass fluxes  $\mathcal{F}_j$  and  $\mathcal{F}_{j+1}$ , to the velocity field; we set

$$\mathcal{G}_{j+\frac{1}{2}} = u_j \mathcal{F}_{j+\frac{1}{2}}^+ + u_{j+1} \mathcal{F}_{j+\frac{1}{2}}^-. \quad (12)$$

(The scheme designed in [37] adopts a different averaged definition for obtaining the momentum fluxes from the mass fluxes.) Finally, the pressure gradient at  $x_{j+\frac{1}{2}}$  is naturally centred

$$\Pi_{j+\frac{1}{2}} = p(\rho_{j+\frac{1}{2}}). \quad (13)$$

Owing to (8), the momentum flux is consistent. Without source terms, the scheme can be shown to preserve the positivity of the density and the entropy dissipation property

under a suitable CFL condition [10], it is thus consistent with the Euler system [9]. For the source term, a natural approach consists in setting

$$S_j = \rho_j \frac{z_{j+\frac{1}{2}} - z_{j-\frac{1}{2}}}{\delta x_j}.$$

Unfortunately this definition does not produce satisfactory results, since it is not consistent with the equilibrium solution (see Remark 2.2 for further comments, describing a specific situation – for the Shallow-Water equation and the fluxes of [37] – where such a definition is well-balanced, though).

## 2.2 Incorporation of the source terms

According to [12] and [5, 6, 7, 13], we introduce hydrostatic reconstructions of the density, compatible with the equilibrium, defined at the interfaces  $x_j$  (see Fig. 2) by setting

$$\begin{aligned} z_j &= \max(z_{j+\frac{1}{2}}, z_{j-\frac{1}{2}}), \\ \mathcal{E}(\rho_j^r) &= [\mathcal{E}(\rho_{j+\frac{1}{2}}) + z_{j+\frac{1}{2}} - z_j]_+, \\ \mathcal{E}(\rho_j^\ell) &= [\mathcal{E}(\rho_{j-\frac{1}{2}}) + z_{j-\frac{1}{2}} - z_j]_+. \end{aligned} \tag{14}$$

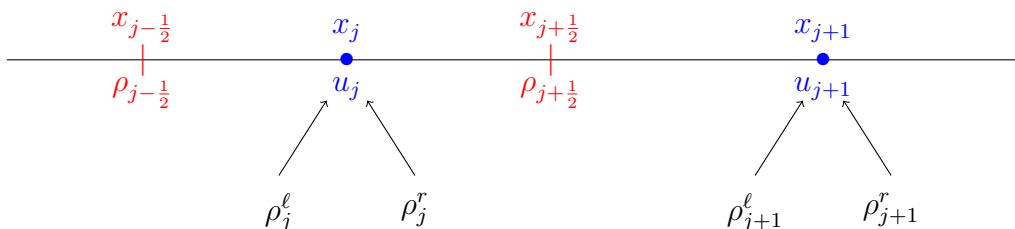


Figure 2: Reconstruction of a WB density.

It is important to note that, as proved in the sequel, these two reconstructions  $\rho_j^r$  and  $\rho_j^\ell$  are equal if the system is at an equilibrium state. Accordingly, it allows us to exactly preserve equilibrium states when proceeding as follows. With these quantities  $\rho_j^\ell$  and  $\rho_j^r$  at hand, we replace the definition of the mass flux in (5) by

$$\mathcal{F}_j^+ = \mathcal{F}^+(\rho_j^\ell, u_j) \quad \text{and} \quad \mathcal{F}_j^- = \mathcal{F}^-(\rho_j^r, u_j),$$

which still accounts for the upwinding principles. For the momentum, we proceed as follows:

- the convection fluxes are defined with these reconstructed mass fluxes, by using (10) and (12),
- the pressure gradient uses the centered definition based on the reconstructed densities

$$p(\rho_j^r) - p(\rho_j^\ell).$$

The non-conservative source term is embodied in this definition.

Thus, we introduce the following mass fluxes, momentum convection fluxes, and the source term

$$\begin{aligned}\mathcal{F}_j &= \mathcal{F}^+(\rho_j^\ell, u_j) + \mathcal{F}^-(\rho_j^r, u_j), \\ \mathcal{G}_{j+\frac{1}{2}} &= \frac{u_j}{2} \left( \mathcal{F}^+(\rho_j^\ell, u_j) + \mathcal{F}^+(\rho_{j+1}^\ell, u_{j+1}) \right) + \frac{u_{j+1}}{2} \left( \mathcal{F}^-(\rho_j^r, u_j) + \mathcal{F}^-(\rho_{j+1}^r, u_{j+1}) \right), \\ S_j &= p(\rho_j^r) - p(\rho_{j+\frac{1}{2}}) - p(\rho_j^\ell) + p(\rho_{j-\frac{1}{2}}).\end{aligned}$$

The well-balanced scheme reads

$$\begin{aligned}\bar{\rho}_{j+\frac{1}{2}} &= \rho_{j+\frac{1}{2}} - \frac{\delta t}{\delta x_{j+\frac{1}{2}}} \left( \mathcal{F}_{j+1} - \mathcal{F}_j \right), \\ \bar{\rho}_j \bar{u}_j &= \rho_j u_j - \frac{\delta t}{\delta x_j} \left( \left( \mathcal{G}_{j+\frac{1}{2}} + \Pi_{j+\frac{1}{2}} \right) - \left( \mathcal{G}_{j-\frac{1}{2}} + \Pi_{j-\frac{1}{2}} \right) + S_j \right),\end{aligned}\tag{15}$$

with  $\Pi_{j+\frac{1}{2}} = p(\rho_{j+\frac{1}{2}})$ .

**Consistency.** The consistency with the exact fluxes comes directly from the consistency of  $\mathcal{F}_j$  and  $\mathcal{G}_{j+\frac{1}{2}}$ . Indeed, if  $z_{j-\frac{1}{2}} = z_{j+\frac{1}{2}} = z_{j+\frac{3}{2}}$  then we have  $\rho_j^r = \rho_{j+\frac{1}{2}}$ ,  $\rho_j^\ell = \rho_{j-\frac{1}{2}}$  and  $\rho_{j+1}^r = \rho_{j+\frac{3}{2}}$ ,  $\rho_{j+1}^\ell = \rho_{j+\frac{1}{2}}$ , so that, in this case,  $\mathcal{F}_j = \mathcal{F}_j$  and  $\mathcal{G}_{j+\frac{1}{2}} = \mathcal{G}_{j+\frac{1}{2}}$ . More interestingly,  $S_j/\delta x_j$  is consistent with the source term  $\rho \partial_x z$ . Let us denote by  $\delta z_j$  the quantity  $z_{j+\frac{1}{2}} - z_{j-\frac{1}{2}}$ . If  $z$  is a regular function this quantity is of order  $\delta x_j$ . We first investigate the specific case of the Shallow-Water system far from dry/wet transition (more precisely assuming that  $\min(\rho_{j-\frac{1}{2}}, \rho_{j+\frac{1}{2}}) \geq |\delta z_j|$  holds). We get

$$\text{(SW)} \quad S_j = \frac{1}{2}(\rho_j^r - \rho_{j+\frac{1}{2}})(\rho_j^r + \rho_{j+\frac{1}{2}}) - \frac{1}{2}(\rho_j^\ell - \rho_{j-\frac{1}{2}})(\rho_j^\ell + \rho_{j-\frac{1}{2}})$$

where the equilibrium relations cast as

$$\text{(SW)} \quad \rho_j^r = \rho_{j+\frac{1}{2}} - [\delta z_j]_-, \quad \rho_j^\ell = \rho_{j-\frac{1}{2}} - [\delta z_j]_+.$$

Hence, we obtain

$$\text{(SW)} \quad S_j = \frac{\rho_{j+\frac{1}{2}} + \rho_{j-\frac{1}{2}}}{2} \delta z_j - \frac{\rho_j^r - \rho_j^\ell}{2} |\delta z_j|.\tag{16}$$

It follows that  $S_j$  is (first order) consistent with  $\rho \partial_x z$ . In the general case, the consistency with the source term comes from the following expansion. As for the case of Shallow-Water equations, the expression of  $\rho_j^r$  and  $\rho_j^\ell$  depends on the sign of  $\delta z_j$ . If  $\delta z_j \geq 0$ , we have the exact equality  $\rho_j^r = \rho_{j+\frac{1}{2}}$ . But, if  $\delta z_j \leq 0$ , we have  $\rho_j^r = \mathcal{E}^{-1}([\mathcal{E}(\rho_{j+\frac{1}{2}}) + \delta z_j]_+)$ . Thus, when  $\delta z_j \leq 0$ , in the case where  $\mathcal{E}(\rho_{j+\frac{1}{2}}) \leq -\delta z_j$ , we have  $\rho_j^r = 0$  whereas, in the case where  $\mathcal{E}(\rho_{j+\frac{1}{2}}) \geq -\delta z_j$ , a Taylor expansion leads to

$$\rho_j^r = \rho_{j+\frac{1}{2}} + \delta z_j \frac{\rho_{j+\frac{1}{2}}}{p'(\rho_{j+\frac{1}{2}})} + o(|\delta z_j|), \quad (\text{when } \delta z_j \leq 0 \text{ and } \mathcal{E}(\rho_{j+\frac{1}{2}}) \geq -\delta z_j),$$

since  $(\mathcal{E}^{-1})'(\mathcal{E}(\rho)) = \frac{\rho}{p'(\rho)}$ . Finally, we have

$$\rho_j^r = \begin{cases} 0, & \text{if } \delta z_j \leq 0 \text{ and } \mathcal{E}(\rho_{j+\frac{1}{2}}) \leq |\delta z_j|, \\ \rho_{j+\frac{1}{2}} + \delta z_j \frac{\rho_{j+\frac{1}{2}}}{p'(\rho_{j+\frac{1}{2}})} + o(|\delta z_j|), & \text{if } \delta z_j \leq 0 \text{ and } \mathcal{E}(\rho_{j+\frac{1}{2}}) \geq |\delta z_j|, \\ \rho_{j+\frac{1}{2}}, & \text{if } \delta z_j \geq 0, \end{cases} \quad (17)$$

and, similarly,

$$\rho_j^\ell = \begin{cases} \rho_{j-\frac{1}{2}}, & \text{if } \delta z_j \leq 0, \\ \rho_{j-\frac{1}{2}} - \delta z_j \frac{\rho_{j-\frac{1}{2}}}{p'(\rho_{j-\frac{1}{2}})} + o(|\delta z_j|), & \text{if } \delta z_j \geq 0 \text{ and } \mathcal{E}(\rho_{j-\frac{1}{2}}) \geq |\delta z_j|, \\ 0, & \text{if } \delta z_j \geq 0 \text{ and } \mathcal{E}(\rho_{j-\frac{1}{2}}) \leq |\delta z_j|. \end{cases} \quad (18)$$

Following the same lines, since

$$(p \circ \mathcal{E}^{-1})'(\mathcal{E}(\rho)) = \rho \quad \text{and} \quad (p \circ \mathcal{E}^{-1})''(\mathcal{E}(\rho)) = \frac{\rho}{p'(\rho)},$$

we have the following expressions for  $p(\rho_j^r)$  and  $p(\rho_j^\ell)$

$$p(\rho_j^r) = \begin{cases} 0, & \text{if } \delta z_j \leq 0 \text{ and } \mathcal{E}(\rho_{j+\frac{1}{2}}) \leq |\delta z_j|, \\ p(\rho_{j+\frac{1}{2}}) + \delta z_j \rho_{j+\frac{1}{2}} + \frac{\delta z_j^2}{2} \frac{\rho_{j+\frac{1}{2}}}{p'(\rho_{j+\frac{1}{2}})} + o(|\delta z_j|^2), & \text{if } \delta z_j \leq 0 \text{ and } \mathcal{E}(\rho_{j+\frac{1}{2}}) \geq |\delta z_j|, \\ p(\rho_{j+\frac{1}{2}}), & \text{if } \delta z_j \geq 0, \end{cases} \quad (19)$$

and

$$p(\rho_j^\ell) = \begin{cases} p(\rho_{j-\frac{1}{2}}), & \text{if } \delta z_j \leq 0, \\ p(\rho_{j-\frac{1}{2}}) - \delta z_j \rho_{j-\frac{1}{2}} + \frac{\delta z_j^2}{2} \frac{\rho_{j-\frac{1}{2}}}{p'(\rho_{j-\frac{1}{2}})} + o(|\delta z_j|^2), & \text{if } \delta z_j \geq 0 \text{ and } \mathcal{E}(\rho_{j-\frac{1}{2}}) \geq |\delta z_j|, \\ 0, & \text{if } \delta z_j \geq 0 \text{ and } \mathcal{E}(\rho_{j-\frac{1}{2}}) \leq |\delta z_j|. \end{cases} \quad (20)$$

We observe that the case where  $p(\rho_j^r) = 0$  occurs only when  $\rho_{j+\frac{1}{2}}$  is sufficiently small since, in this case,  $\rho_{j+\frac{1}{2}} \leq \mathcal{E}^{-1}(|\delta z_j|) \xrightarrow{\delta x \rightarrow 0} 0$ . Moreover, an expansion of  $p(\rho_{j+\frac{1}{2}})$  in this case shows that

$$\begin{aligned} p(\rho_{j+\frac{1}{2}}) &= p \circ \mathcal{E}^{-1}(\mathcal{E}(\rho_{j+\frac{1}{2}})) \\ &= p \circ \mathcal{E}^{-1}(0) + (p \circ \mathcal{E}^{-1})'(0) \mathcal{E}(\rho_{j+\frac{1}{2}}) + o(|\mathcal{E}(\rho_{j+\frac{1}{2}})|) \\ &= o(|\mathcal{E}(\rho_{j+\frac{1}{2}})|). \end{aligned} \quad (21)$$

This proves that, in the case where  $\mathcal{E}(\rho_{j+\frac{1}{2}}) \leq |\delta z_j|$ , we have

$$p(\rho_{j+\frac{1}{2}}) + \delta z_j \rho_{j+\frac{1}{2}} = o(|\delta z_j|).$$

Thus, we finally have

$$p(\rho_j^r) = \begin{cases} p(\rho_{j+\frac{1}{2}}) + \delta z_j \rho_{j+\frac{1}{2}} + o(|\delta z_j|), & \text{if } \delta z_j \leq 0, \\ p(\rho_{j+\frac{1}{2}}), & \text{if } \delta z_j \geq 0, \end{cases}$$

and similarly

$$p(\rho_j^\ell) = \begin{cases} p(\rho_{j-\frac{1}{2}}), & \text{if } \delta z_j \leq 0, \\ p(\rho_{j-\frac{1}{2}}) - \delta z_j \rho_{j-\frac{1}{2}} + o(|\delta z_j|), & \text{if } \delta z_j \geq 0, \end{cases}$$

It leads to the following equality for  $S_j$

$$S_j = \begin{cases} \delta z_j \rho_{j+\frac{1}{2}} + o(|\delta z_j|), & \text{if } \delta z_j \leq 0, \\ \delta z_j \rho_{j-\frac{1}{2}} + o(|\delta z_j|), & \text{if } \delta z_j \geq 0. \end{cases}$$

The term  $S_j/\delta x_j$  is thus consistent with  $\rho \partial_x z$ .

**Remark 2.1.** Far from wet/dry transition (when  $\min(\mathcal{E}(\rho_{j-\frac{1}{2}}), \mathcal{E}(\rho_{j+\frac{1}{2}})) \geq |\delta z_j|$ ) a first order consistency error is obtained. Moreover, it also applies in dry area if  $\lim_{\rho \rightarrow 0} p''(\rho) \neq 0$  since in this case, the  $o(|\mathcal{E}(\rho_{j+\frac{1}{2}})|)$  in (21) is actually a  $O(|\mathcal{E}(\rho_{j+\frac{1}{2}})|^2)$ .

**Preservation of equilibrium state.** A key property of the construction is the equality  $\rho_j^r = \rho_j^\ell$  at equilibrium. Indeed, by definition of the equilibrium state (2) associated to the constant  $\eta$ , we have

$$\mathcal{E}(\rho_{j\pm\frac{1}{2}}) + z_{j\pm\frac{1}{2}} = \max(z_{j\pm\frac{1}{2}}, \eta),$$

so that, since  $z_j = \max(z_{j-\frac{1}{2}}, z_{j+\frac{1}{2}})$ , at the equilibrium state we have

$$\mathcal{E}(\rho_j^r) = \mathcal{E}(\rho_j^\ell) = [\eta - z_j]_+.$$

It ensures the equality  $\rho_j^r = \rho_j^\ell$ . Note that the positive part in the definition (14) of  $\rho_j^r$  and  $\rho_j^\ell$  is crucial to ensure the equality  $\rho_j^r = \rho_j^\ell$  in the dry area (where  $z_j > \eta$ ).

Thus, if the system is at an equilibrium state, that is, in particular,  $\rho_{j-\frac{1}{2}} = \hat{\rho}_{j-\frac{1}{2}}$ ,  $\rho_{j+\frac{1}{2}} = \hat{\rho}_{j+\frac{1}{2}}$ ,  $\rho_{j+\frac{3}{2}} = \hat{\rho}_{j+\frac{3}{2}}$ ,  $u_j = 0$ ,  $u_{j-1} = 0$  and  $u_{j+1} = 0$ , as mentioned above, we have  $\rho_j^r = \rho_j^\ell$  and  $\rho_{j+1}^r = \rho_{j+1}^\ell$ . Thus, the mass fluxes vanish at  $x_{j+\frac{1}{2}}$  and  $x_{j-\frac{1}{2}}$  since, by consistency of the splitting, they are equal to  $\rho_{j+1}^r u_{j+1} = \rho_{j+1}^\ell u_{j+1} = 0$  and  $\rho_j^r u_j = \rho_j^\ell u_j = 0$  respectively. The density remains unchanged. Since  $u_j = 0$ ,  $u_{j-1} = 0$  and  $u_{j+1} = 0$ , the momentum fluxes vanish and the sum of the pressure and source term which is equal to  $p(\rho_j^r) - p(\rho_j^\ell)$  is also zero since  $\rho_j^r = \rho_j^\ell$ . The velocity remains unchanged and the equilibrium states are perfectly preserved.

**Remark 2.2** (A simple staggered WB scheme for the Shallow-Water system, [24]). For the Shallow-Water system, the following simple staggered scheme, proposed in [24], based on the upwinding according to the material velocity as in [37]

$$\begin{aligned}
\bar{\rho}_{j+\frac{1}{2}} &= \rho_{j+\frac{1}{2}} - \frac{\delta t}{\delta x_{j+\frac{1}{2}}} \underbrace{\left( [u_{j+1}]_+ \rho_{j+\frac{1}{2}} + [u_{j+1}]_- \rho_{j+\frac{3}{2}} \right)}_{\mathcal{F}_{j+1}} \\
&\quad - \frac{\delta t}{\delta x_{j+\frac{1}{2}}} \underbrace{\left( [u_j]_+ \rho_{j-\frac{1}{2}} + [u_j]_- \rho_{j+\frac{1}{2}} \right)}_{\mathcal{F}_j}, \\
\bar{\rho}_j \bar{u}_j &= \rho_j u_j - \frac{\delta t}{2\delta x_j} \left( u_j [\mathcal{F}_j + \mathcal{F}_{j+1}]_+ + u_{j+1} [\mathcal{F}_j + \mathcal{F}_{j+1}]_- \right) \\
&\quad - \frac{\delta t}{2\delta x_j} \left( u_{j-1} [\mathcal{F}_{j-1} + \mathcal{F}_j]_+ + u_j [\mathcal{F}_{j-1} + \mathcal{F}_j]_- \right) \\
&\quad - \frac{\delta t}{\delta x_j} (p(\rho_{j+\frac{1}{2}}) - p(\rho_{j-\frac{1}{2}})) - \frac{\delta t}{\delta x_j} (\rho_{j+\frac{1}{2}} + \rho_{j-\frac{1}{2}}) \frac{z_{j+\frac{1}{2}} - z_{j-\frac{1}{2}}}{2}
\end{aligned} \tag{22}$$

is well-balanced in the case where there is no dry area. If  $(\hat{\rho}_{j+\frac{1}{2}}, \hat{u}_j)$  is an equilibrium state with no dry area (see (2) with  $\eta > \max_j (z_{j+\frac{1}{2}})$ ), the mass fluxes and the convection fluxes vanish since  $\hat{u}_j = 0$ , while the last two terms of the momentum equation in (22) recombine as  $\frac{\hat{\rho}_{j+\frac{1}{2}} + \hat{\rho}_{j-\frac{1}{2}}}{2} ((\hat{\rho}_{j+\frac{1}{2}} + z_{j+\frac{1}{2}}) - (\hat{\rho}_{j-\frac{1}{2}} + z_{j-\frac{1}{2}}))$ . Away from wet/dry transition, this term vanishes too. Note that the well-balanced property of the scheme (22) in this case crucially relies on the specific form of both the numerical fluxes and of the pressure law.

**Stability analysis.** The numerical scheme should at least preserve the positivity of the density, which can be seen as a minimal stability criterion. To this end, we observe that  $\rho \mapsto \mathcal{E}(\rho)$  is non decreasing. Hence, since  $z_j \geq z_{j\pm\frac{1}{2}}$ , we have  $\mathcal{E}(\rho_{j+1}^\ell) \leq \mathcal{E}(\rho_{j+\frac{1}{2}})$ ,  $\mathcal{E}(\rho_j^r) \leq \mathcal{E}(\rho_{j+\frac{1}{2}})$  and thus  $\rho_{j+1}^\ell \leq \rho_{j+\frac{1}{2}}$ ,  $\rho_j^r \leq \rho_{j+\frac{1}{2}}$ . The monotonicity of the flux function leads to  $\mathcal{F}^+(\rho_{j+1}^\ell, u_{j+1}) \leq \mathcal{F}^+(\rho_{j+\frac{1}{2}}, u_{j+1})$  and  $\mathcal{F}^-(\rho_j^r, u_j) \geq \mathcal{F}^-(\rho_{j+\frac{1}{2}}, u_j)$ . Since  $\mathcal{F}^+(\rho_j^\ell, u_j) \geq 0$  and  $-\mathcal{F}^-(\rho_{j+1}^r, u_{j+1}) \geq 0$ , we arrive from (15) at

$$\begin{aligned}
\bar{\rho}_{j+\frac{1}{2}} &\geq \rho_{j+\frac{1}{2}} - \frac{\delta t}{\delta x_{j+\frac{1}{2}}} \mathcal{F}^+(\rho_{j+1}^\ell, u_{j+1}) + \frac{\delta t}{\delta x_{j+\frac{1}{2}}} \mathcal{F}^-(\rho_j^r, u_j) \\
&\geq \rho_{j+\frac{1}{2}} - \frac{\delta t}{\delta x_{j+\frac{1}{2}}} \mathcal{F}^+(\rho_{j+\frac{1}{2}}, u_{j+1}) + \frac{\delta t}{\delta x_{j+\frac{1}{2}}} \mathcal{F}^-(\rho_{j+\frac{1}{2}}, u_j).
\end{aligned}$$

We can now conclude as in [10, Prop. 3.7]: under the CFL-condition

$$\frac{\delta t}{\delta x_{j+\frac{1}{2}}} \left( [\lambda_+(\rho_{j+\frac{1}{2}}, u_{j+1})]_+ + [\lambda_-(\rho_{j+\frac{1}{2}}, u_j)]_- \right) \leq 1$$

the scheme (15) preserves the positivity of the discrete density.

### 2.3 Second order version of the WB scheme

We propose a second-order accurate version of the scheme. To this end, we make use of the principles of the MUSCL methods [53]. For the source-free problem, we refer the reader to [31] for the adaptation of this framework to the scheme described in Section 2.1. Let us denote

$$W = \mathcal{E}(\rho) + z$$

the quantity conserved by the equilibrium. The idea is to introduce a  $\mathbb{P}1$  interpolation of the numerical unknowns in order to define new interface values. Namely, we set

$$\rho_j^- = \rho_{j-\frac{1}{2}} + \pi_{j-\frac{1}{2}}(x_j - x_{j-\frac{1}{2}}), \quad \rho_j^+ = \rho_{j+\frac{1}{2}} + \pi_{j+\frac{1}{2}}(x_j - x_{j+\frac{1}{2}}),$$

and we proceed similarly with

$$W_j^- = W_{j-\frac{1}{2}} + \tilde{\pi}_{j-\frac{1}{2}}(x_j - x_{j-\frac{1}{2}}), \quad W_j^+ = W_{j+\frac{1}{2}} + \tilde{\pi}_{j+\frac{1}{2}}(x_j - x_{j+\frac{1}{2}}).$$

In these formula,  $\pi_{j+\frac{1}{2}}, \tilde{\pi}_{j+\frac{1}{2}}$  are some appropriately defined slopes, that accounts for a limitation mechanism in order to prevent under/overshoots in the vicinity of shocks; in such regions the scheme degrades to first order. The design of limiters is completely standard; we refer the reader to [31] and the references therein for further details. We reconstruct an interface data for the bottom topography by introducing

$$z_j^- = W_j^- - \mathcal{E}(\rho_j^-), \quad z_j^+ = W_j^+ - \mathcal{E}(\rho_j^+).$$

Next, we set

$$z_j^{ml} = \max(z_j^-, z_j^+),$$

bearing in mind that these reconstructed quantities might vary at each time step, while the force density  $z$  does not depend on time. Finally, we reconstruct the interface densities by using the same idea as before, using the interpolated values

$$\begin{aligned} \mathcal{E}(\rho_j^{ml,r}) &= [\mathcal{E}(\rho_j^+) + z_j^+ - z_j^{ml}]_+ = [W_j^+ - z_j^{ml}]_+, \\ \mathcal{E}(\rho_j^{ml,\ell}) &= [\mathcal{E}(\rho_j^-) + z_j^- - z_j^{ml}]_+ = [W_j^- - z_j^{ml}]_+. \end{aligned}$$

The mass fluxes are then set to

$$\mathcal{F}_j^{ml} = \mathcal{F}^+(\rho_j^{ml,\ell}, u_j) + \mathcal{F}^-(\rho_j^{ml,r}, u_j).$$

For the momentum equation, we similarly reconstruct a velocity

$$u_{j+\frac{1}{2}}^- = u_j + \nu_j(x_{j+\frac{1}{2}} - x_j), \quad u_{j+\frac{1}{2}}^+ = u_{j+1} + \nu_{j+1}(x_{j+\frac{1}{2}} - x_{j+1}),$$

where  $\nu_j$  are convenient slopes defined from limiters. We then adapt accordingly the definition of the convection fluxes:

$$\begin{aligned} \mathcal{G}_{j+\frac{1}{2}}^{ml} &= \frac{u_{j+\frac{1}{2}}^-}{2} \left( \mathcal{F}^+(\rho_j^{ml,\ell}, u_j) + \mathcal{F}^+(\rho_{j+1}^{ml,\ell}, u_{j+1}) \right) \\ &\quad + \frac{u_{j+\frac{1}{2}}^+}{2} \left( \mathcal{F}^-(\rho_j^{ml,r}, u_j) + \mathcal{F}^-(\rho_{j+1}^{ml,r}, u_{j+1}) \right). \end{aligned}$$

The centered approximation of the pressure with

$$\Pi_{j+\frac{1}{2}} = p(\rho_{j+\frac{1}{2}})$$

gives a second order approximation. What is more subtle is the treatment of the source terms. So far, we have just replaced  $\rho_j^{r/\ell}$  (or  $u_j$ ) by the values  $\rho_j^{ml,r/\ell}$  (or  $u_{j\pm\frac{1}{2}}^\mp$ ) obtained by using the limited interpolation. Proceeding similarly with the source term produces an approximation which is not consistent (essentially since the reconstructions  $z_j^\pm$  used in the definition of  $\rho_j^{ml,r/\ell}$  are two (second order) approximations of  $z$  at the same point  $x_j$ ). A further inspection of formula (16) shows that the obstacle for having a second order approximation seems to come from the term

$$\frac{\rho_j^r - \rho_j^\ell}{2} |\delta z_j|$$

By the way, the scheme discussed in Remark 2.2 precisely disregard this term. This suggests that we should stick to the definition of the source term with (14) and just correct the first order defect; namely, we use

$$S_j^{ml} = p(\rho_j^r) - p(\rho_{j+\frac{1}{2}}) - p(\rho_j^\ell) + p(\rho_{j-\frac{1}{2}}) + \frac{\rho_j^r - \rho_j^\ell}{2} |\delta z_j|. \quad (23)$$

The scheme thus reads

$$\begin{aligned} \bar{\rho}_{j+\frac{1}{2}} &= \rho_{j+\frac{1}{2}} - \frac{\delta t}{\delta x_{j+\frac{1}{2}}} \left( \mathcal{F}_{j+1}^{ml} - \mathcal{F}_j^{ml} \right), \\ \bar{\rho}_j \bar{u}_j &= \rho_j u_j - \frac{\delta t}{\delta x_j} \left( \left( \mathcal{G}_{j+\frac{1}{2}}^{ml} + \Pi_{j+\frac{1}{2}} \right) - \left( \mathcal{G}_{j-\frac{1}{2}}^{ml} + \Pi_{j-\frac{1}{2}} \right) + S_j^{ml} \right), \end{aligned}$$

with  $\Pi_{j+\frac{1}{2}} = p(\rho_{j+\frac{1}{2}})$ .

**Consistency.** For the Shallow-Water system (when  $\min(\rho_{j-\frac{1}{2}}, \rho_{j+\frac{1}{2}}) \geq |\delta z_j|$ ), (23) exactly casts as

$$\text{(SW)} \quad S_j^{ml} = \frac{\rho_{j+\frac{1}{2}} + \rho_{j-\frac{1}{2}}}{2} (z_{j+\frac{1}{2}} - z_{j-\frac{1}{2}}).$$

We recover the treatment of the pressure gradient/source term devised in Remark 2.2, which is indeed a second order approximation of  $\rho \partial_x z$  at  $x_j$ . Hence, for reaching the second order accuracy, we remove from the centered well-balanced formula  $p(\rho_j^r) - p(\rho_{j+\frac{1}{2}}) - p(\rho_j^\ell) + p(\rho_{j-\frac{1}{2}})$  the correction term  $(\rho_j^r - \rho_j^\ell) |\delta z_j|/2$  (which produces a  $O(1)$  error). This simple approach applies to more general pressure laws. We are led to evaluate the consistency error of

$$S_j^{ml} = (p(\rho_j^r) - p(\rho_{j+\frac{1}{2}})) - (p(\rho_j^\ell) - p(\rho_{j-\frac{1}{2}})) - \frac{1}{2} (\rho_j^r - \rho_j^\ell) |\delta z_j|.$$

We go back to (17), (18), (19) and (20) to obtain the following expansions

$$p(\rho_j^r) - p(\rho_{j+\frac{1}{2}}) + \frac{1}{2}\rho_j^r|\delta z_j| = \begin{cases} -p(\rho_{j+\frac{1}{2}}), & \text{if } \delta z_j \leq 0 \text{ and } \mathcal{E}(\rho_{j+\frac{1}{2}}) \leq |\delta z_j|, \\ \frac{1}{2}\delta z_j \rho_{j+\frac{1}{2}} + o(|\delta z_j|^2), & \text{if } \delta z_j \leq 0 \text{ and } \mathcal{E}(\rho_{j+\frac{1}{2}}) \geq |\delta z_j|, \\ \frac{1}{2}\delta z_j \rho_{j+\frac{1}{2}}, & \text{if } \delta z_j \geq 0, \end{cases}$$

$$p(\rho_j^\ell) - p(\rho_{j-\frac{1}{2}}) + \frac{1}{2}\rho_j^\ell|\delta z_j| = \begin{cases} -\frac{1}{2}\rho_{j-\frac{1}{2}}\delta z_j, & \text{if } \delta z_j \leq 0, \\ -\frac{1}{2}\rho_{j-\frac{1}{2}}\delta z_j + o(|\delta z_j|^2), & \text{if } \delta z_j \geq 0 \text{ and } \mathcal{E}(\rho_{j-\frac{1}{2}}) \geq |\delta z_j|, \\ -p(\rho_{j-\frac{1}{2}}), & \text{if } \delta z_j \geq 0 \text{ and } \mathcal{E}(\rho_{j-\frac{1}{2}}) \leq |\delta z_j|. \end{cases}$$

Bearing in mind that, in the case where  $\mathcal{E}(\rho_{j\pm\frac{1}{2}}) \leq |\delta z_j|$ , we have

$$p(\rho_{j\pm\frac{1}{2}}) + \delta z_j \rho_{j\pm\frac{1}{2}} = o(|\delta z_j|),$$

we obtain

$$S_j = \begin{cases} \frac{1}{2}(\rho_{j-\frac{1}{2}} + \rho_{j+\frac{1}{2}})\delta z_j + o(|\delta z_j|), & \text{if } \min(\mathcal{E}(\rho_{j-\frac{1}{2}}), \mathcal{E}(\rho_{j+\frac{1}{2}})) \leq |\delta z_j|, \\ \frac{1}{2}(\rho_{j-\frac{1}{2}} + \rho_{j+\frac{1}{2}})\delta z_j + o(|\delta z_j|^2), & \text{otherwise.} \end{cases}$$

The term  $\frac{1}{2}(\rho_{j-\frac{1}{2}} + \rho_{j+\frac{1}{2}})\delta z_j/\delta x_j$  provides a second order accurate approximation of the source term  $\rho\partial_x z$  at the point  $x_j$ . Thus,  $S_j/\delta x_j$  can reach a second order accuracy away from dry/wet transition (more precisely when  $\min(\mathcal{E}(\rho_{j-\frac{1}{2}}), \mathcal{E}(\rho_{j+\frac{1}{2}})) \geq |\delta z_j|$ ).

**Preservation of equilibrium state.** Equilibrium states (2) with no dry area (that is  $W_{j+\frac{1}{2}} = \eta$ ) are preserved by the MUSCL reconstruction (*i.e.*  $W_j^\pm = \eta$ ) and, as proved in the previous Section, we then obtain  $\rho_j^r = \rho_j^\ell$  and  $\rho_j^{ml,r} = \rho_j^{ml,\ell}$ . It readily follows that the second order version of the scheme preserves equilibrium with no dry area. In the presence of dry area, the preservation of equilibrium states is also valid. However, the MUSCL reconstruction no longer exactly preserves the equilibrium states near wet/dry transitions. Nevertheless we can observe, thanks to the properties of the reconstruction that  $W_j^\pm \geq \eta$ , since at equilibrium we have  $W_{j+\frac{1}{2}} = \max(\eta, z_{j+\frac{1}{2}}) \geq \eta$ . Moreover, we have

$$W_{j+\frac{1}{2}} = \eta \implies (W_j^+ = \eta, W_{j+1}^- = \eta)$$

$$W_{j+\frac{1}{2}} = z_{j+\frac{1}{2}} \implies (\rho_j^+ = 0, \rho_{j+1}^- = 0).$$

Indeed, when  $W_{j+\frac{1}{2}} = \eta$ , we necessarily have  $W_{j-\frac{1}{2}} \geq W_{j+\frac{1}{2}}$  and  $W_{j+\frac{3}{2}} \geq W_{j+\frac{1}{2}}$ , so that the properties of the slope-limiter implies that  $\tilde{\pi}_{j+\frac{1}{2}} = 0$ , ensuring the asserted property. The second line is similarly obtained since when  $W_{j+\frac{1}{2}} = z_{j+\frac{1}{2}}$ , we have

$\rho_{j+\frac{1}{2}} = 0 \leq \min(\rho_{j-\frac{1}{2}}, \rho_{j+\frac{3}{2}})$  so that  $\pi_{j+\frac{1}{2}} = 0$ . With these properties at hand, it is now straightforward to prove that  $\rho_j^{ml,r} = \rho_j^{ml,\ell}$ . Indeed, we distinguish four cases. First, if  $W_{j-\frac{1}{2}} = \eta$  and  $W_{j+\frac{1}{2}} = \eta$  then we have  $W_j^\pm = \eta$  which leads to the equality  $\rho_j^{ml,r} = \rho_j^{ml,\ell}$ . If  $W_{j-\frac{1}{2}} = z_{j-\frac{1}{2}}$  and  $W_{j+\frac{1}{2}} = z_{j+\frac{1}{2}}$  then  $\rho_j^\pm$  vanish, so that  $z_j^\pm = W_j^\pm$  and the equality  $\rho_j^{ml,r} = \rho_j^{ml,\ell}$  still holds. Finally the two last cases are symmetric. For instance, if  $W_{j-\frac{1}{2}} = z_{j-\frac{1}{2}}$  and  $W_{j+\frac{1}{2}} = \eta$  then we have  $\rho_j^- = 0$  and  $W_j^+ = \eta$ . This implies that  $\eta \leq W_j^- = z_j^- \leq z_j^{ml}$ . Thus,  $\rho_j^{ml,r}$  and  $\rho_j^{ml,\ell}$  both vanish in this case. The equality  $\rho_j^{ml,r} = \rho_j^{ml,\ell}$  is ensured in the four possible cases and, as previously, it guarantees that the second order version of the scheme preserves the equilibrium states (2).

### 3 Numerical experiments

To illustrate the ability of the proposed approach in handling balance laws with complex source terms, we challenge the scheme against several benchmark tests, in 1D and 2D. The presented simulations are performed for the Shallow-Water equation ( $\gamma = 2$ ), written in the form

$$\begin{aligned} \partial_t \rho + \partial_x(\rho u) &= 0, \\ \partial_t(\rho u) + \partial_x(\rho u^2 + g\rho^2/2) &= -g\rho \partial_x z \end{aligned} \quad (24)$$

with  $g > 0$ , the gravity constant, for the sake of comparison, but it also applies for general pressure laws. For all the 1D simulations, the time step is fixed at each time iteration by imposing the following equality

$$\delta t = C_{\delta t} \frac{\delta x}{\max_j |u_j| + \max_j c(\rho_{j+1/2})}$$

where  $C_{\delta t}$  is a constant whose value is made precise in the description of each test case.

#### 3.1 Lake at rest

We first check that the order 1 and order 2 schemes solve exactly the lake at rest solutions. The computational domain is  $[0, 20]$ . We choose a bottom topography with a parabolic obstacle defined by

$$z(x) = \begin{cases} 0.2 - 0.05(x - 10)^2, & \text{if } 8 < x < 12, \\ 0, & \text{otherwise.} \end{cases}$$

The initial velocity is set to zero and the initial height is set to

$$\rho(x) = \begin{cases} 0.1 - z(x), & \text{if } x < 10 - \sqrt{2} \text{ or } x > 10 + \sqrt{2}, \\ 0, & \text{otherwise,} \end{cases}$$

so that the free surface is horizontal and there is a dry zone at the top of the obstacle for  $x$  between  $10 - \sqrt{2}$  and  $10 + \sqrt{2}$ . The initial data is a stationary solution of the problem. The final time of the simulation is set to  $T = 1000$  and  $C_{\delta t}$  is set to 0.9. We observe that the schemes (first and second order versions) exactly preserve the initial state whatever is the mesh size ( $\delta x = 1, 0.1, 0.01$ ).

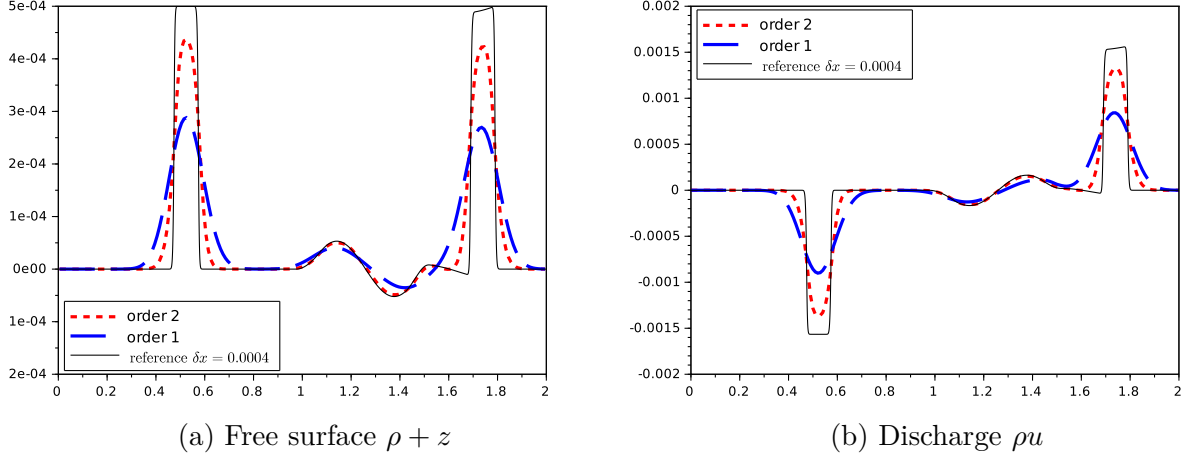


Figure 3: Perturbations of the lake at rest: numerical solutions obtained for  $\delta x = 0.01$

### 3.2 Perturbations of the lake at rest solution

Referring to [45] (see also [7, 16]), we investigate the propagation of small perturbations of the lake at rest steady solution. The computational domain is now the interval  $[0, 2]$  and the gravity constant is  $g = 9.8$ . The bottom topography is defined by

$$z(x) = \begin{cases} -1 + 0.25 \left( 1 + \cos(10\pi(x - 0.5)) \right), & \text{if } 1.4 < x < 1.6, \\ -1, & \text{otherwise.} \end{cases}$$

The steady state solution is a flat free surface at rest. It is perturbed by a pulse and two opposite waves appear over the bump. The initial data are given by

$$u(x) = 0, \quad \forall x \in [0, 2], \quad \text{and} \quad \rho(x) = \begin{cases} -z(x) + 0.001, & \text{if } 1.4 < x < 1.6, \\ -z(x), & \text{otherwise.} \end{cases}$$

The final time of the simulation is set to  $T = 0.2$  and  $C_{\delta t}$  is set to 0.5. The numerical results are presented in Fig. 3 (the free surface at left and the discharge  $q = \rho u$  at right). A reference solution is computed with  $\delta x = 4 \times 10^{-4}$ , it is plotted in black solid line. The numerical results obtained with  $\delta x = 10^{-2}$  are plotted in blue dashed line for the first order scheme and in red dotted line for the second order scheme. The results are comparable to those obtained in the literature and we clearly see the advantage of running the second order scheme.

### 3.3 Flow over an isolated bump

In this Section, we consider flows governed by Shallow-Water equations, over an isolated convex obstacle which is assumed to be symmetric with respect to its crest. The flow goes from the left to the right. Its velocity and height far from the obstacle are denoted by  $u_0 > 0$  and  $\rho_0$ . A transient motion develops at the obstacle and moves in both directions. After sufficient time has elapsed, the flow reaches a steady state

in the vicinity of the obstacle; transient structures move away from the obstacle and reach asymptotic states. The asymptotic states can be entirely characterized from the values of  $u_0$  and  $\rho_0$  and the geometry of the bump, as it is fully detailed in [40]. For the sake of completeness, we recall here the different situations which can occur and how the asymptotic reference solution can be computed in the different cases. Let us denote by  $F_0$  be the Froude number computed from  $u_0$  and  $\rho_0$ :

$$F_0 = \frac{u_0}{\sqrt{g\rho_0}},$$

while  $Z_c$  stands for the height of the obstacle crest. We distinguish two situations depending on the values of the coefficient

$$M_0 = \frac{1}{2}F_0^2 - \frac{3}{2}F_0^{2/3} + 1$$

compared to the normalized height of the obstacle crest

$$M_c = \frac{Z_c}{\rho_0}.$$

In the case where

$$M_c < M_0,$$

the flow reaches a steady state. More precisely, when  $F_0 < 1$  the free surface at the steady state dips symmetrically over the symmetrical obstacle (see Fig. 4a) whereas when  $F_0 > 1$  the steady state rises over the obstacle (see Fig. 4b). The reference solution can be obtained by solving the steady state equations

$$\begin{cases} \frac{u^2}{2g} + \rho + z = \text{constant}_1, \\ \rho u = \text{constant}_2. \end{cases}$$

Using the background state  $(\rho_0, u_0)$  far from the obstacle, we can thus obtain  $\rho$  from

$$\frac{\rho_0^2 u_0^2}{2g\rho^2} + \rho + z = \frac{u_0^2}{2g} + \rho_0,$$

and then  $u = \rho_0 u_0 / \rho$ . Note that  $\rho$  and  $u$  depends on the space variable  $x$  since in these equations  $z$  is a function of  $x$ .

The situation is more intricate when

$$M_c > M_0.$$

The obstacle partially blocks the flow, a bore forms around the obstacle and the flow becomes discontinuous, hydraulic jumps appear. A discontinuity appears downstream the obstacle and propagates towards the left. The flow is sonic at the crest of the obstacle, that is, denoting  $(\rho_c, u_c)$  the flow state at the crest of the obstacle, we have  $u_c = \sqrt{g\rho_c}$ . Upstream the obstacle, two slightly different situations can asymptotically occur. In the first case, a discontinuity appears after the obstacle and propagates

towards the right (see Fig. 4c) whereas in the second case, a stationary shock lies above the obstacle (see Fig. 4d). In both cases, a rarefaction wave allows the flow to go back to the background state  $(\rho_0, u_0)$ . The asymptotic reference solution can be obtained as follows. We denote by  $(\rho_A, u_A)$  the constant state reached after the downstream hydraulic jump (before the obstacle). It is linked to the background state  $(\rho_0, u_0)$  by the following Rankine-Hugoniot condition

$$\rho_A u_A = \rho_A u_0 + (\rho_0 - \rho_A) \sqrt{\frac{g}{2} \frac{\rho_A}{\rho_0} (\rho_0 + \rho_A)}.$$

Moreover, it is also linked to the state above the obstacle by steady state equations

$$\begin{cases} \frac{u_A^2}{2g} + \rho_A = \frac{u_c^2}{2g} + \rho_c + Z_c, \\ \rho_A u_A = \rho_c u_c. \end{cases}$$

Thus, since  $\rho_c u_c = \sqrt{g} \rho_c^{3/2}$ ,  $\rho_A$  can be obtained by solving

$$\rho_c^3 + 2\rho_A^2 = (3\rho_c + 2Z_c)\rho_A^2,$$

where

$$\rho_c = \left( \rho_A \frac{u_0}{\sqrt{g}} + (\rho_0 - \rho_A) \sqrt{\frac{g}{2} \frac{\rho_A}{\rho_0} (\rho_0 + \rho_A)} \right)^{\frac{2}{3}}.$$

Next, we compute the asymptotic reference solution after the bore. We first assume that we are in the situation where an hydraulic jump propagates away from the obstacle. We are led to compute two constant states to compute  $(\rho_B, u_B)$  and  $(\rho_x, u_x)$  (see Fig 4c). The states  $(\rho_c, u_c)$  and  $(\rho_B, u_B)$  are linked by steady states equations

$$\rho_c^3 + 2\rho_B^2 = (3\rho_c + 2Z_c)\rho_B^2, \quad (\rho_B \neq \rho_A).$$

It allows us to compute  $\rho_B$  since now  $\rho_c$  is known. Then  $u_B = \rho_c u_c / \rho_B$ . Next, the states  $(\rho_B, u_B)$  and  $(\rho_x, u_x)$  are linked by the Rankine-Hugoniot condition

$$\rho_B u_B = \rho_B u_x + (\rho_x - \rho_B) \sqrt{\frac{g}{2} \frac{\rho_B}{\rho_x} (\rho_x + \rho_B)}$$

Finally, the states  $(\rho_x, u_x)$  and  $(\rho_0, u_0)$  are linked by a rarefaction wave so that the Riemann invariants are preserved

$$u_x - 2\sqrt{g\rho_x} = u_0 - 2\sqrt{g\rho_0}.$$

Thus,  $\rho_x$  can be obtained by solving

$$\rho_B u_B = \rho_B \left( u_0 - 2\sqrt{g\rho_0} + 2\sqrt{g\rho_x} \right) + (\rho_x - \rho_B) \sqrt{\frac{g}{2} \frac{\rho_B}{\rho_x} (\rho_x + \rho_B)}.$$

The displacement velocity of the shock is  $(\rho_x u_x - \rho_B u_B) / (\rho_x - \rho_B)$ . We distinguish now two cases: if this velocity is positive the shock propagates away from the obstacle

and we have obtained the asymptotic reference solution (see Fig 4c); if this velocity is negative, the obtained solution is not physically relevant and should be disregarded. We have to construct a solution with a stationary shock above the obstacle. In this case, we are left with the task of determining three states  $(\rho_-, u_-)$ ,  $(\rho_+, u_+)$  and  $\rho_x, u_x$  (see Fig 4d). The states  $(\rho_A, u_A)$  and  $(\rho_-, u_-)$  are linked by steady state equations

$$\begin{cases} \frac{u_-^2}{2g} + \rho_- + Z_* = \frac{u_A^2}{2g} + \rho_A, \\ \rho_- u_- = \rho_A u_A, \end{cases}$$

where  $Z_*$  stands for the height of the obstacle at the shock position. The states  $(\rho_-, u_-)$  and  $(\rho_+, u_+)$  are linked by the Rankine-Hugoniot conditions for a stationary shock

$$\begin{cases} \rho_- u_- = \rho_+ u_+, \\ \rho_+ u_+ - \sqrt{\frac{g}{2} \rho_+ \rho_- (\rho_- + \rho_+)} = 0. \end{cases}$$

The states  $(\rho_+, u_+)$  and  $(\rho_x, u_x)$  are linked by steady state equations

$$\begin{cases} \frac{u_+^2}{2g} + \rho_+ + Z_* = \frac{u_x^2}{2g} + \rho_x, \\ \rho_+ u_+ = \rho_x u_x. \end{cases}$$

Finally, as before, the states  $(\rho_x, u_x)$  and  $(\rho_0, u_0)$  are linked by a rarefaction wave

$$u_x - 2\sqrt{g\rho_x} = u_0 - 2\sqrt{g\rho_0}.$$

Thus, we deal with the four following equations

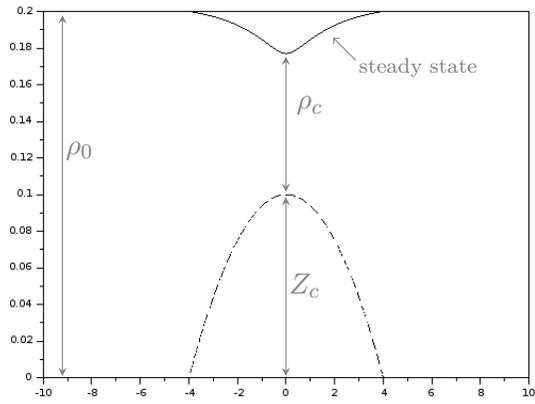
$$\begin{cases} \frac{\rho_A^2 u_A^2}{2g\rho_-^2} + \rho_- + Z_* = \frac{u_A^2}{2g} + \rho_A, \\ \rho_A u_A - \sqrt{\frac{g}{2} \rho_+ \rho_- (\rho_- + \rho_+)} = 0 \\ \frac{\rho_A^2 u_A^2}{2g\rho_+^2} + \rho_+ + Z_* = \frac{\rho_A^2 u_A^2}{2g\rho_x^2} + \rho_x, \\ \frac{\rho_A u_A}{\rho_x} - 2\sqrt{g\rho_x} = u_0 - 2\sqrt{g\rho_0}, \end{cases}$$

to determine  $\rho_-, \rho_+, \rho_x$  and  $Z_*$ .

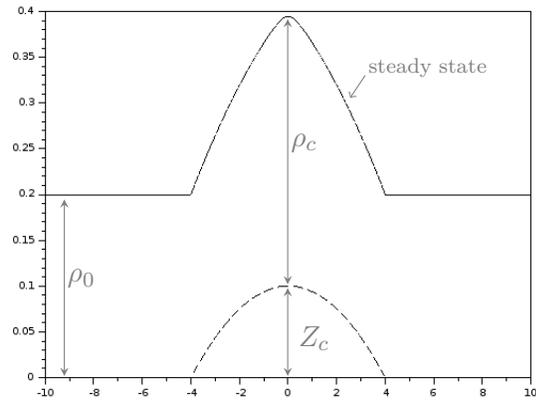
In conclusion, there exists four different classes of asymptotic solutions as illustrated in Fig. 4. We numerically investigate these cases. The obstacle is defined by

$$z(x) = \frac{1}{10} \left( 1 - \frac{x^2}{16} \right),$$

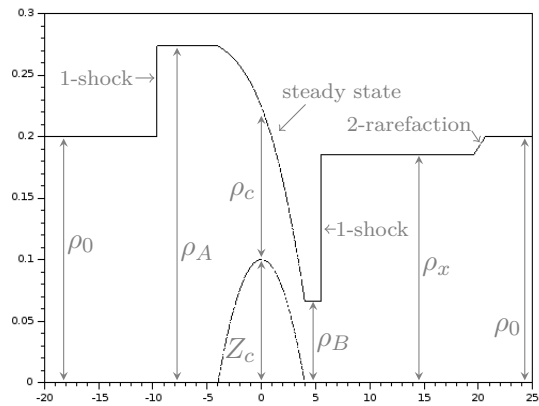
so that  $Z_c = 0.1$ . We fix  $\rho_0 = 0.2$  and compute the velocity  $u_0$  from different values of  $F_0 = 0.2, 0.3, 0.7, 1.9$ , the gravity  $g$  being fixed to 9.8. In these test cases, we set  $C_{\delta t} = 0.5$ .



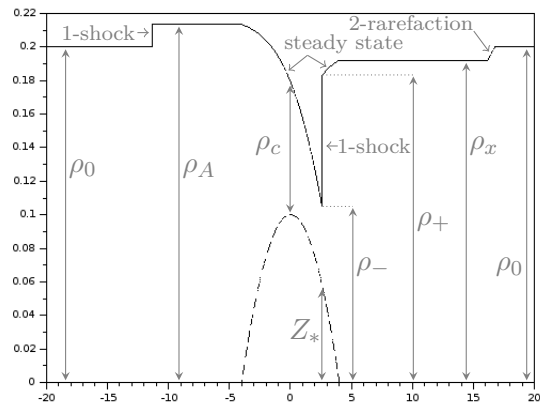
(a)  $M_c < M_0$  and  $F_0 > 1$



(b)  $M_c < M_0$  and  $F_0 > 1$



(c)  $M_c > M_0$ , upstream moving shock.



(d)  $M_c > M_0$ , stationary shock.

Figure 4: Flow over an isolated obstacle: structure of the asymptotic solution. Free surface (solid lines) and obstacle (dotted lines)

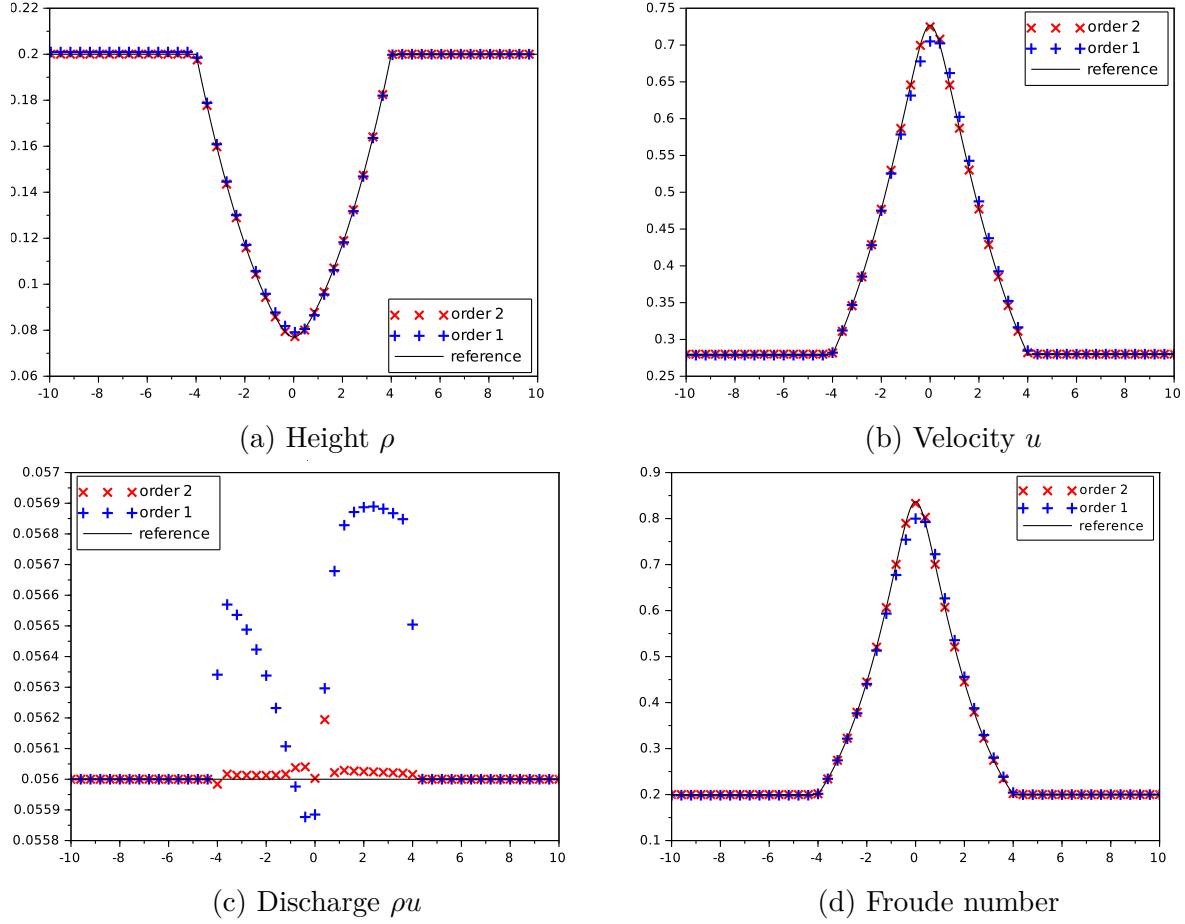
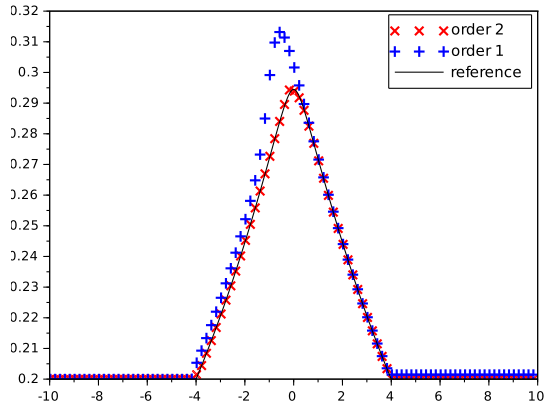


Figure 5: Flow over an isolated obstacle: numerical solutions obtained for  $F_0 = 0.2$ ,  $\delta x = 0.05$  at  $T = 2000$

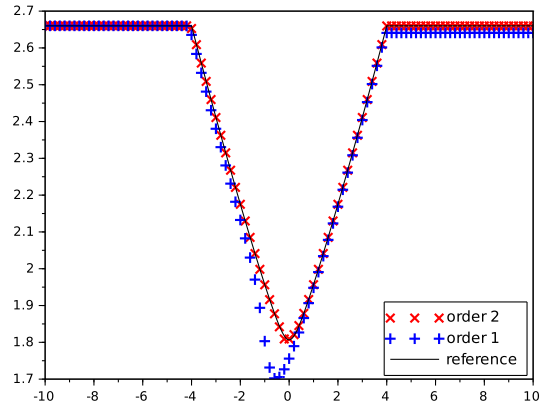
### 3.3.1 Cases $F_0 = 0.2$ and $F_0 = 1.9$

In these two cases, we have  $M_c < M_0$ . As expected, the numerical solutions reach a steady state. The results obtained at time  $T = 2000$  with our schemes (order 1 and order 2) are presented in Fig. 5 and Fig. 6 for  $\delta x = 0.05$ . We obtain a good agreement with the reference profile computed with the procedure explained above. In the case  $F_0 = 0.2$ , the free surface dips over the obstacle whereas in the case  $F_0 = 1.0$ , it rises over the bump.

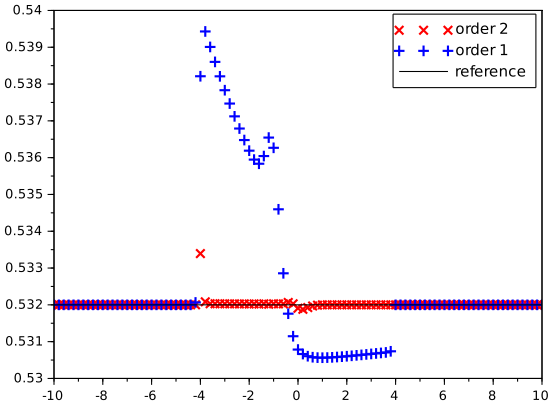
In Fig. 7, we present the discrete error in  $L^1$ -norm as a function of the mesh size. As expected, we observe that the MUSCL reconstruction procedure allows to reach the second order accuracy for the velocity  $u$  and the height  $h$ .



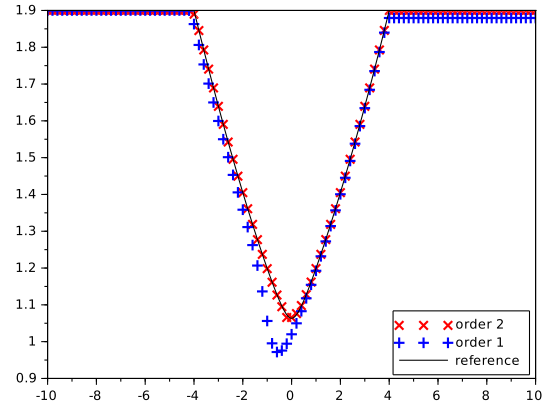
(a) Height  $\rho$



(b) Velocity  $u$



(c) Discharge  $\rho u$



(d) Froude number

Figure 6: Flow over an isolated obstacle: numerical solutions obtained for  $F_0 = 1.9$ ,  $\delta x = 0.04$  at  $T = 2000$

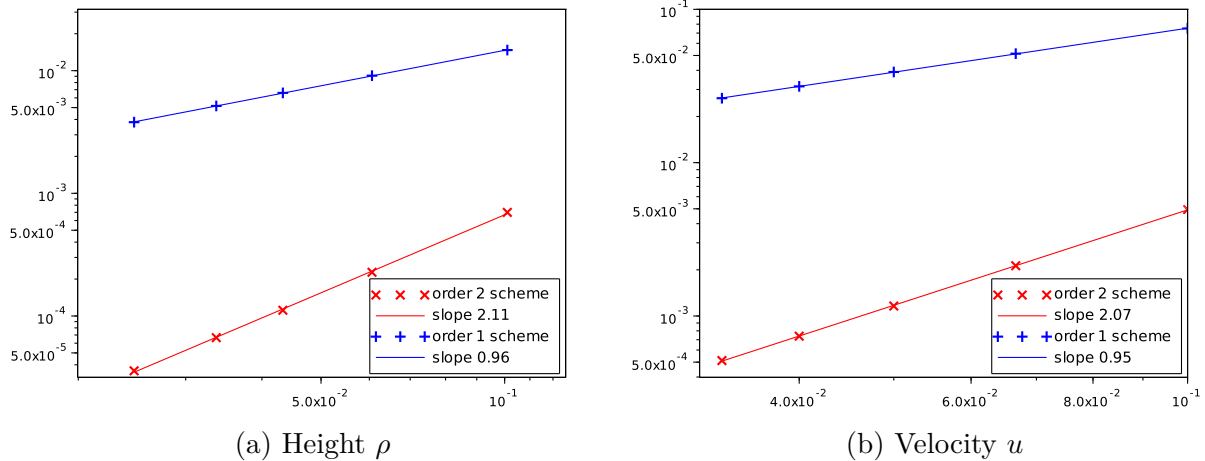


Figure 7: Flow over an isolated obstacle: discrete error in  $L^1$ -norm as a function of the mesh size

### 3.3.2 Case $F_0 = 0.3$

In this case, we have  $M_c > M_0$ , this is the situation illustrated in Fig. 4d. A stationary shock appears behind the obstacle. The result obtained at time  $T = 30$  with our scheme (order 1 and order 2) are presented in Fig. 8 for  $\delta x = 0.1$ . We also represent with a solid line the asymptotic reference profile. We observe that the constant states  $\rho_A$  and  $\rho_+$ , the value  $\rho_-$  and the equilibrium profiles (before and after the stationary shock) perfectly match with the reference profile. However, the numerical solutions at time  $T = 30$  present some additional structures compared to the reference asymptotic solution. These additional structures appear near the upstream shock and near the downstream rarefaction wave. Since the obtained numerical solutions seem to be converged with respect to  $\delta x$  and  $\delta t$ , we guess that we face transient structures that do not appear, by definition, in the asymptotic profile. We plot in Fig. 9 and Fig. 10 a zoom on the structure for three larger final times  $T = 100$ ,  $T = 250$  and  $T = 2000$ . We indeed observe that the bump in Fig. 9 and the oscillations in Fig. 10 vanish as the time increases.

### 3.3.3 Case $F_0 = 0.7$

In this case, we still have  $M_c > M_0$ , but now in the situation of Fig. 4c. The shock which appears behind the obstacle is moving to the right. The results obtained at time  $T = 30$  with our schemes (order 1 and order 2) are presented in Fig. 11 for  $\delta x = 0.1$ . We also represent with a solid line the asymptotic reference profile. Again, we observe that the constant states  $\rho_A$ ,  $\rho_B$ ,  $\rho_x$  and the equilibrium profile perfectly match with the reference profile. The position of the shocks is also in agreement with the reference asymptotic solution. As previously, at time  $T = 30$ , we also observe an additional transient structure in the numerical solutions compared to the reference asymptotic solution in the neighborhood of the rarefaction wave.

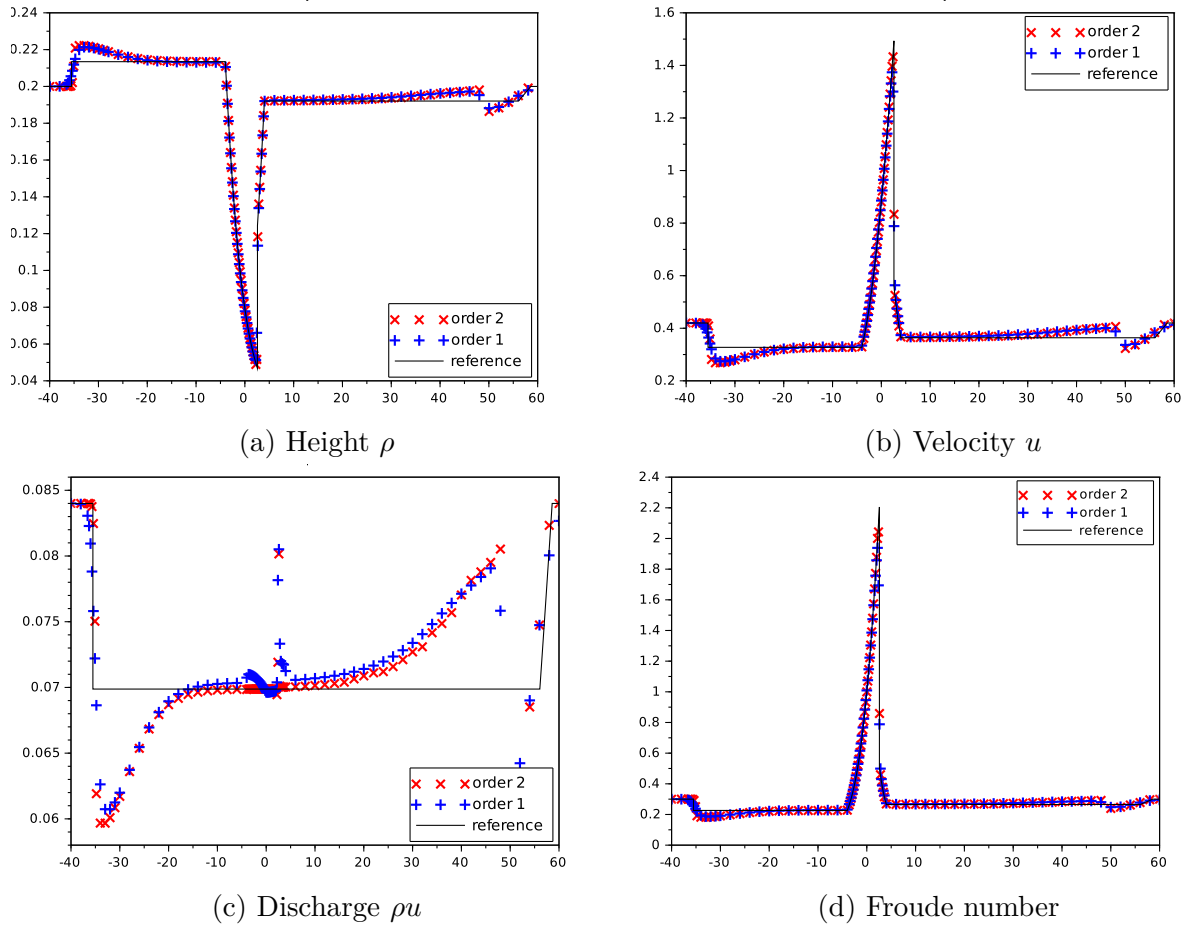


Figure 8: Flow over an isolated obstacle: numerical solutions obtained for  $F_0 = 0.3$ ,  $\delta x = 0.1$  at  $T = 30$

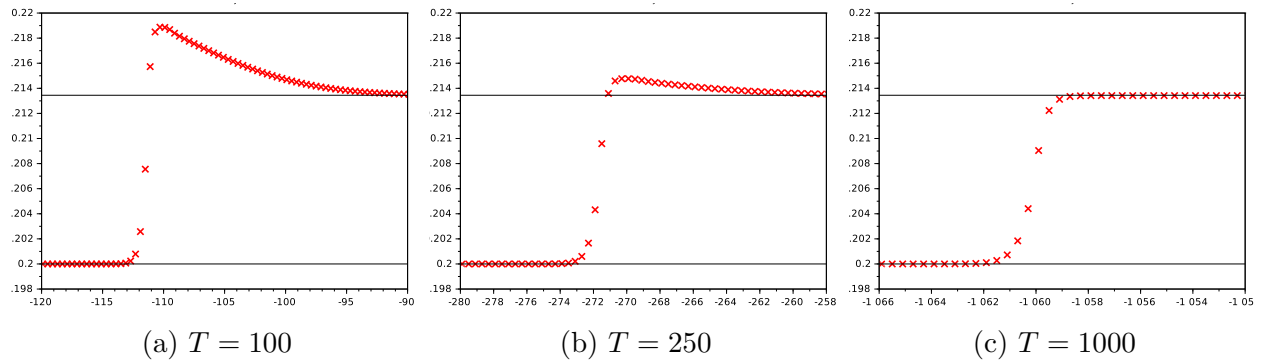


Figure 9: Flow over an isolated obstacle: numerical solutions obtained for  $F_0 = 0.3$ ,  $\delta x = 0.2$ , zoom on the density

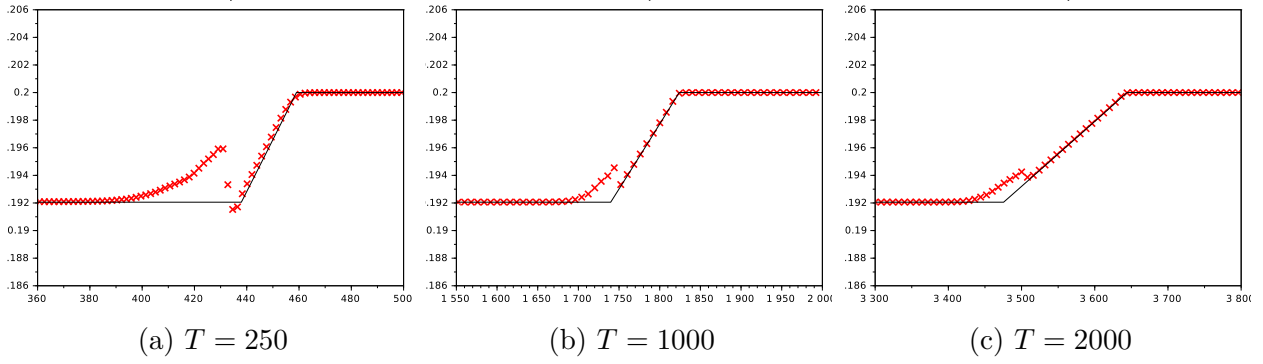


Figure 10: Flow over an isolated obstacle: numerical solutions obtained for  $F_0 = 0.3$ ,  $\delta x = 0.2$ , zoom on the density

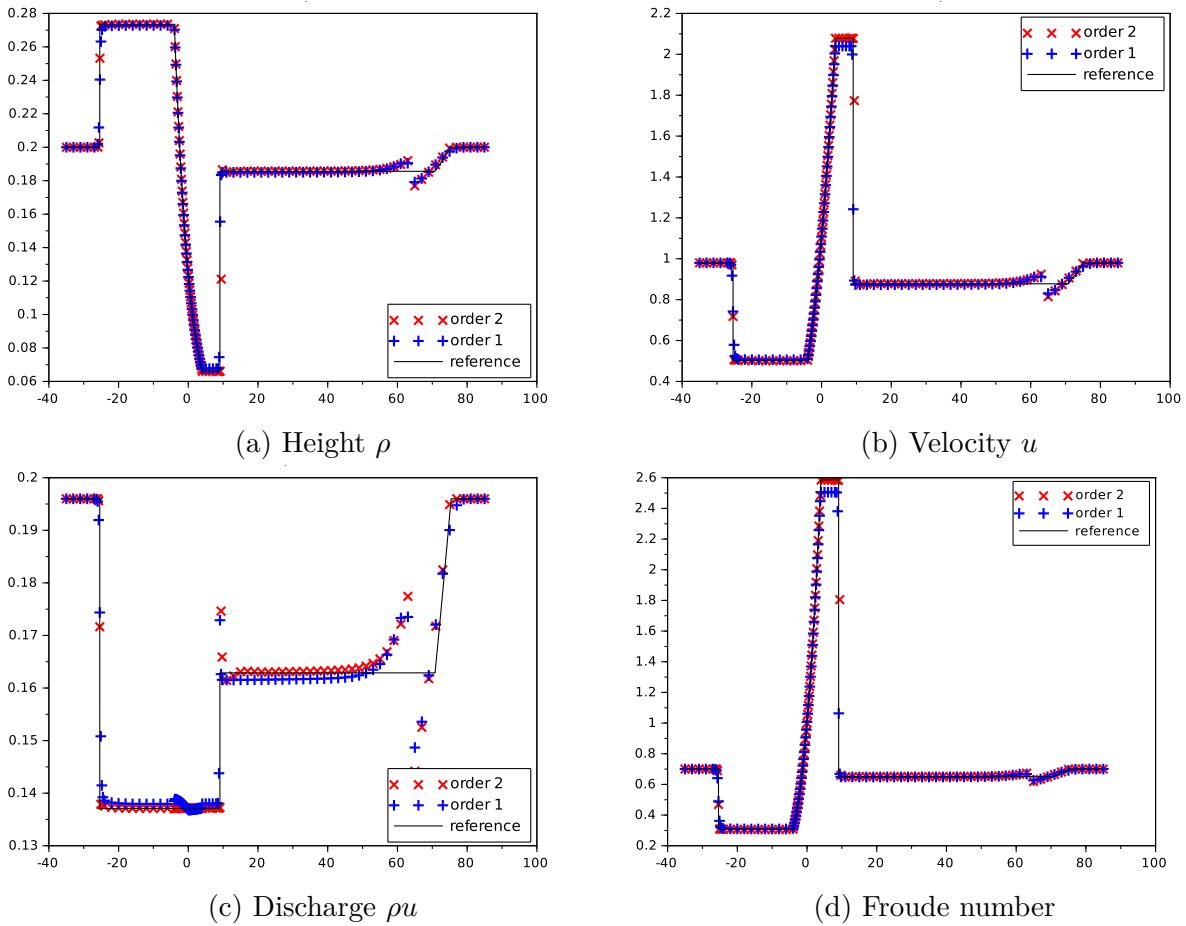


Figure 11: Flow over an isolated obstacle: numerical solutions obtained for  $F_0 = 0.7$ ,  $\delta x = 0.1$  at  $T = 30$

### 3.4 Wet/dry fronts in a nonflat bassin

We consider in this Section a test case proposed by [25] (see also [7, 16]). The computational domain is  $[0, 25]$  and the gravity is  $g = 9.8$ . The bottom topography is defined by

$$z(x) = \begin{cases} -13, & \text{if } 25/3 < x < 25/2, \\ -14, & \text{otherwise.} \end{cases}$$

With  $q = \rho u$ , the initial data are given by

$$\rho(x) = -z(x) - 4, \quad \text{and} \quad q(x) = \begin{cases} -350, & \text{if } x \leq 50/3, \\ 350, & \text{if } x > 50/3. \end{cases}$$

We use  $\delta x = 5 \times 10^{-3}$  and  $C_{\delta t} = 0.4$ . The numerical solution obtained with our schemes are presented in Fig. 12 (for the first order scheme) and in Fig. 13 (for the second order scheme) at different times  $t = 0.05$ ,  $t = 0.25$  and  $t = 0.45$ . Two rarefaction waves propagate in opposite directions creating a dry bed. The schemes capture correctly the generation and propagation of the wet-dry fronts (even when the wave propagates over the step).

### 3.5 Thacker test: oscillation in a 2D-paraboloid

In this Section, we consider the 2D problem of a free surface oscillating in a paraboloid [50, 20, 21]. The computational domain is  $[-2, 2] \times [-2, 2]$ . The topography is given by

$$z(x, y) = \frac{1}{2}(x^2 + y^2 - 1).$$

The initial data are given by

$$\begin{aligned} \rho(x, y) &= (0.125 * (4x - 1) - z(x, y)) \mathbb{1}_{(x-0.5)^2 + y^2 < 1}, \\ u(x, y) &= \begin{pmatrix} 0 \\ 0.5 \end{pmatrix} \times \mathbb{1}_{(x-0.5)^2 + y^2 < 1}. \end{aligned}$$

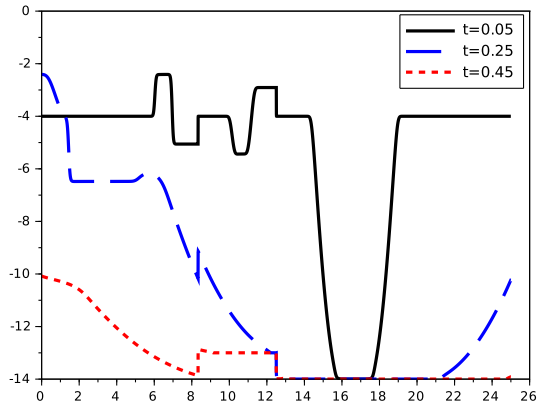
This is a planar free surface with a non-vanishing initial velocity. The solution is exactly known; it is given by

$$\begin{cases} \rho(t, x, y) = (0.125(4x \cos(t) + 4y \sin(t) - 1) - z(x, y)) \mathbb{1}_{(x-0.5 \cos(t))^2 + (y-0.5 \sin(t))^2 < 1}, \\ u(t, x, y) = \frac{1}{2} \begin{pmatrix} -\sin(t) \\ \cos(t) \end{pmatrix}. \end{cases}$$

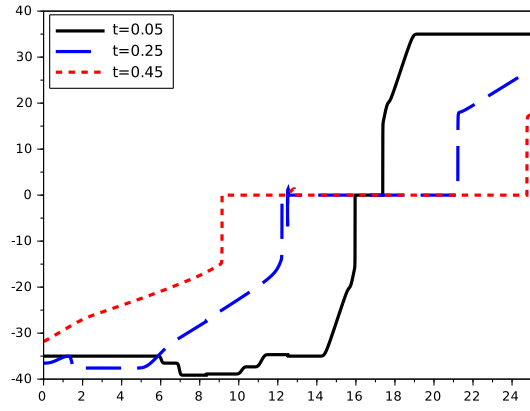
The solution is  $2\pi$ -periodic with respect to the time variable. The free surface remains planar in time with a moving circular wet/dry transition line. The numerical results obtained with the first and second order schemes are presented in Fig. 14 and 15. For this test case, the time step is defined by

$$\delta t = 0.2 \min(\delta x, \delta y).$$

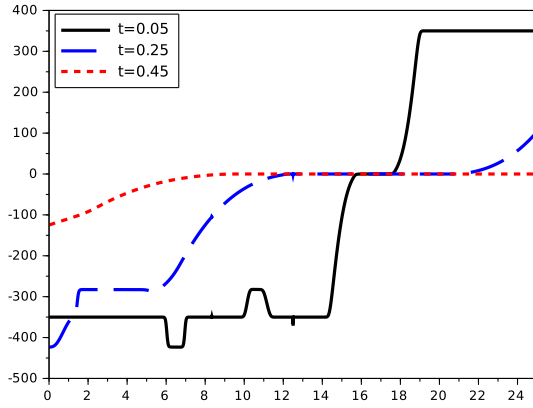
Figure 14 shows the discrete error in  $L^1$ -norm at time  $T = 4\pi$  as a function of the mesh size. As expected, we observe that the MUSCL reconstruction procedure reaches higher



(a) Free surface  $\rho + z$

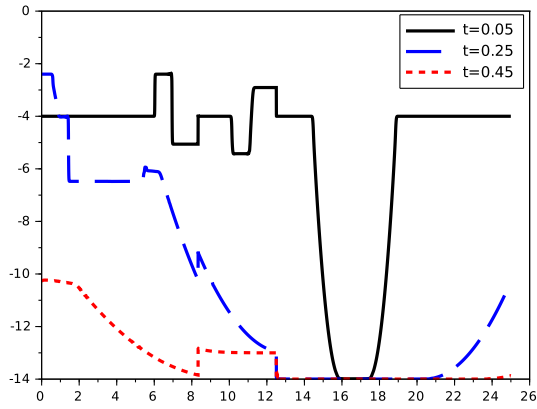


(b) Velocity  $u$

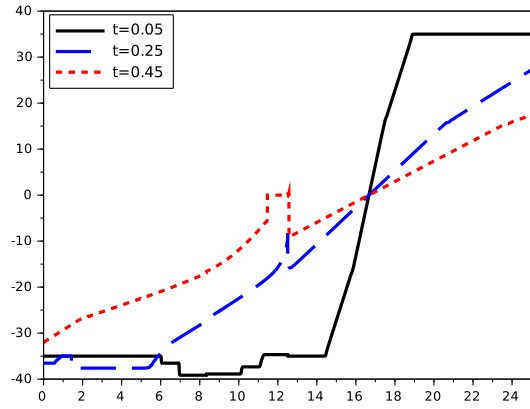


(c) Discharge  $\rho u$

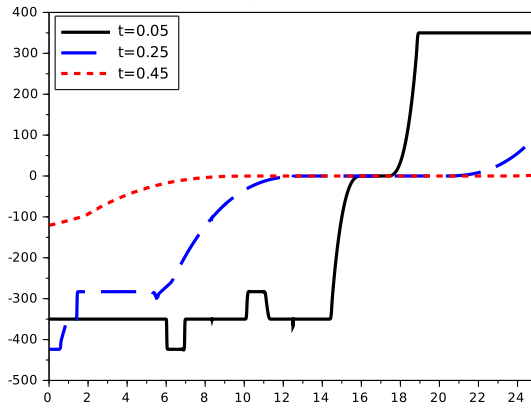
Figure 12: Wet/dry fronts in a nonflat bassin: numerical solutions obtained with the first order scheme,  $\delta x = 0.005$



(a) Free surface  $\rho + z$



(b) Velocity  $u$



(c) Free surface  $\rho u$

Figure 13: Wet/dry fronts in a nonflat basin: numerical solutions obtained with the second order scheme,  $\delta x = 0.005$

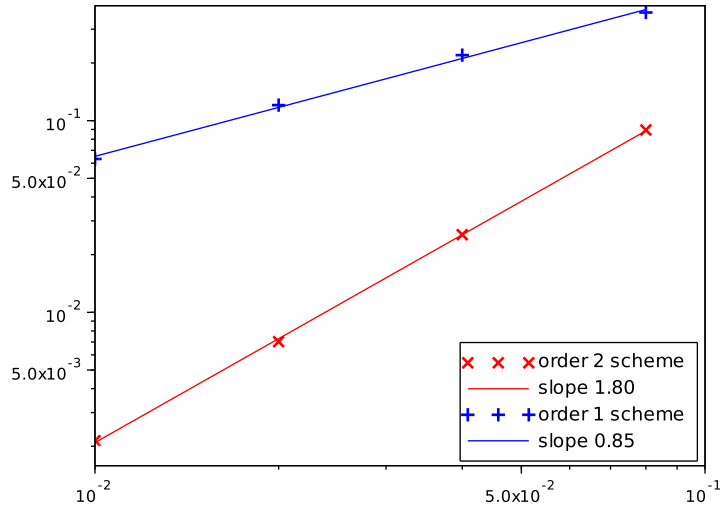


Figure 14: 2D Thacker test: discrete error in  $L^1$ -norm as a function of the mesh size (1st and 2nd order schemes)

accuracy (1.8 convergence order). The approximate solutions obtained at  $T = 4\pi$  with  $\delta x = 0.01$  and  $\delta y = 0.01$  are presented in Fig. 15. At the left, in Fig. 15a, we provide the contour lines of the free surface. We clearly observe the circular shoreline and the planar free surface. In Fig. 15b, we provide a cutline along the axis  $y = 0$  and we compare the results obtained with the first or second order scheme with the reference exact solution.

## References

- [1] CALIF3S, a software components library for the computation of reactive turbulent flows.
- [2] M. V. A. Bermudez. Upwind methods for hyperbolic conservation laws with source terms. *Computers & Fluids*, 23:1049–1071, 1994.
- [3] A. Arakawa and V. R. Lamb. Computational design of the basic dynamical processes of the UCLA general circulation model. *Methods in Computational Physics: Advances in Research and Applications*, 17:173–265, 1977.
- [4] A. Arakawa and V. R. Lamb. A potential enstrophy and energy conserving scheme for the shallow water equations. *Monthly Weather Rev.*, 109(1):18–36, 1981.
- [5] E. Audusse, F. Bouchut, and M.-O. Bristeau. A well-balanced positivity preserving “second-order” scheme for shallow water flows on unstructured meshes. *J. Comput. Phys.*, 206(1):311–333, 2005.

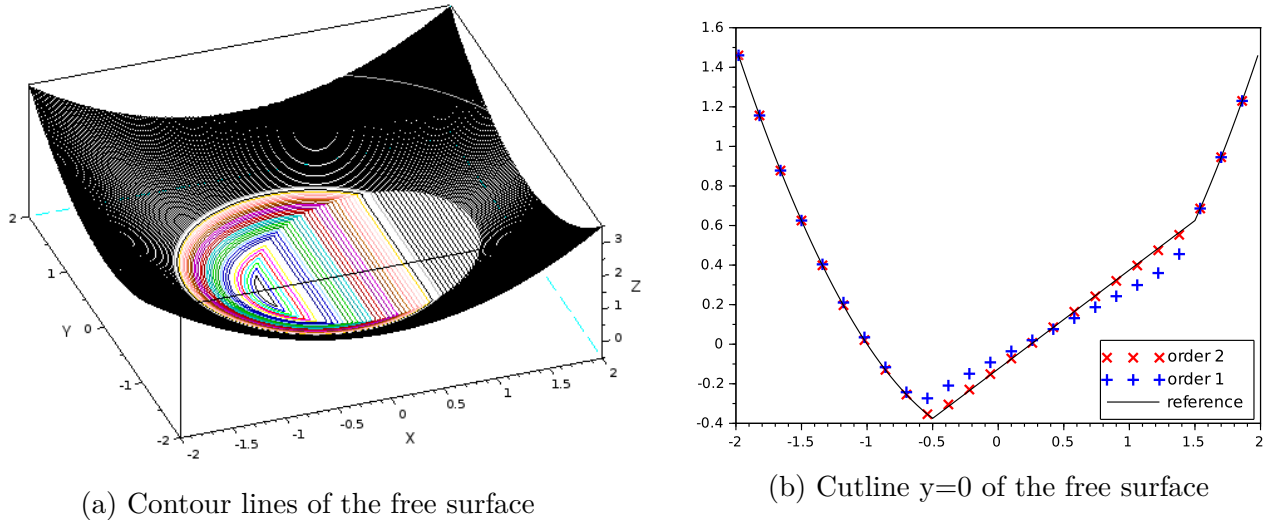


Figure 15: 2D Thacker test: numerical solution obtained with  $\delta x = \delta y = 0.01$  using the 2nd order scheme (left) and comparison of a cutline with the first order scheme

- [6] E. Audusse, F. Bouchut, M.-O. Bristeau, R. Klein, and B. Perthame. A fast and stable well-balanced scheme with hydrostatic reconstruction for shallow water flows. *SIAM J. Sci. Comput.*, 25(6):2050–2065, 2004.
- [7] E. Audusse, C. Chalons, and P. Ung. A simple well-balanced and positive numerical scheme for the shallow-water system. *Comm. Math. Sci.*, 13(5):1317–1332, 2015.
- [8] D. Benson. Computational methods in lagrangian and eulerian hydrocodes. *Comput. Methods Appl. Mech. Eng.*, 99:235–394, 1992.
- [9] F. Berthelin, T. Goudon, and S. Minjeaud. Consistency analysis of a 1D finite volume scheme for barotropic Euler models. In *Finite volumes for complex applications VII. Methods and theoretical aspects*, volume 77 of *Springer Proc. Math. Stat.*, pages 97–105. Springer, Cham, 2014.
- [10] F. Berthelin, T. Goudon, and S. Minjeaud. Kinetic schemes on staggered grids for barotropic Euler models: entropy-stability analysis. *Math. Comp.*, 84(295):2221–2262, 2015.
- [11] F. Berthelin, T. Goudon, and S. Minjeaud. Multifluid flows: a kinetic approach. *J. Sci. Comput.*, 66(2):792–824, 2016.
- [12] R. Botchorishvili, B. Perthame, and A. Vasseur. Equilibrium schemes for scalar conservation laws with stiff sources. *Math. Comp.*, 72(241):131–157, 2003.
- [13] F. Bouchut. *Nonlinear stability of finite volume methods for hyperbolic conservation laws and well-balanced schemes for sources*. Frontiers in Mathematics. Birkhäuser, 2004.
- [14] P. Cargo and A.-Y. LeRoux. Un schéma équilibre adapté au modèle d’atmosphère avec termes de gravité. *C. R. Acad. Sci. Paris Sér. I Math.*, 318(1):73–76, 1994.

- [15] M. Castro, A. Milanés, and C. Pares. Well-balanced numerical schemes based on a generalized hydrostatic reconstruction technique. *Math. Models Methods Appl. Sci.*, 17:2055–2113, 2007.
- [16] M. J. Castro, A. Pardo, C. Parés, and E. F. Toro. On some fast well-balanced first order solvers for nonconservative systems. *Math. Comp.*, 79(271):1427–1472, 2010.
- [17] F. Coron and B. Perthame. Numerical passage from kinetic to fluid equations. *SIAM J. Numer. Anal.*, 28:26–42, 1991.
- [18] C. Dafermos. *Hyperbolic conservation laws in continuum physics*, volume 325 of *Grundlehren der mathematischen Wissenschaften*. Springer, 2010. Third ed.
- [19] G. Dakin, B. Després, and S. Jaouen. High-order staggered schemes for compressible hydrodynamics. weak consistency and numerical validation. *J. Comput. Phys.*, 376:339–364, 2019.
- [20] O. Delestre. *Simulation du ruissellement d’eau de pluie sur des surfaces agricoles*. PhD thesis, Université d’Orléans, 2010.
- [21] O. Delestre, C. Lucas, P.-A. Ksinant, F. Darboux, C. Laguerre, T.-N.-T. Vo, F. James, and S. Cordier. SWASHES: a compilation of shallow water analytic solutions for hydraulic and environmental studies. *Int. J. for Numer. Methods in Fluids*, 72(3):269–300, 2013.
- [22] S. M. Deshpande. Kinetic theory based new upwind methods for inviscid compressible flows. In *AIAA 24th Aerospace Science Meeting, Jan 6-9, 1986, Nevada, USA*, 1986. AIAA paper 86-0275.
- [23] S. M. Deshpande. On the Maxwellian distribution, symmetric form and entropy conservation for the Euler equations. Technical report, NASA Langley Research Centre, Hampton, VA, 1986. NASA TP2613.
- [24] D. Doyen and P. H. Gunawan. An explicit staggered finite volume scheme for the shallow water equations. In *Finite Volumes for Complex Applications VII-Methods and Theoretical Aspects*, volume 77 of *Springer Proceedings in Mathematics & Statistics*. Springer, 2014.
- [25] T. Gallouët, J.-M. Hérard, and N. Seguin. Some approximate Godunov schemes to compute shallow water equations with topography. *Computers & Fluids*, 32:479–513, 05 2003.
- [26] L. Gastaldo, R. Herbin, W. Kheriji, C. Lapuerta, and J.-C. Latché. Staggered discretizations, pressure correction schemes and all speed barotropic flows. In *Finite Volumes for Complex Applications VI, Problems and Perspectives, Prague, Czech Republic*, volume 4, pages 839–855, 2011.
- [27] L. Gastaldo, R. Herbin, J.-C. Latché, and N. Therme. A MUSCL-type segregated-explicit staggered scheme for the Euler equations. *Computers & Fluids*, 175:91–110, 2018.
- [28] E. Godlewski and P.-A. Raviart. *Numerical approximation of hyperbolic systems of conservation laws*, volume 118 of *Applied Mathematical Sciences*. Springer, New-York, 1996.

- [29] L. Gosse. *Computing Qualitatively Correct Approximations of Balance Laws*, volume 2 of *SIMAI Springer Series*. Springer, 2013.
- [30] T. Goudon, J. Llobell, and S. Minjeaud. An asymptotic preserving scheme on staggered grids for the barotropic Euler system in low Mach regimes. *Numer. Methods PDE*, 36(5):1098–1128, 2020.
- [31] T. Goudon, J. Llobell, and S. Minjeaud. An explicit MUSCL scheme on staggered grids with kinetic-like fluxes for the barotropic and full Euler system. *Commun. Comput. Phys.*, 27(3):672–724, 2020.
- [32] T. Goudon, J. Llobell, and S. Minjeaud. An explicit finite volume scheme on staggered grids for the Euler equations: unstructured meshes, stability analysis, and energy conservation. *Internat. J. Numer. Methods Fluids*, 94(1):76–119, 2022.
- [33] J. M. Greenberg and A.-Y. Leroux. A well-balanced scheme for the numerical processing of source terms in hyperbolic equations. *SIAM J. Numer. Anal.*, 33(1):1–16, 1996.
- [34] F. H. Harlow and J. E. Welch. Numerical calculation of time-dependent viscous incompressible flow of fluid with free surface. *Phys. Fluids*, 8(12):2182–2189, 1965.
- [35] R. Herbin, W. Kheriji, and J.-C. Latché. Staggered schemes for all speed flows. *ESAIM:Proc*, 35:122–150, 2012. Actes du Congrès National de Mathématiques Appliquées et Industrielles.
- [36] R. Herbin, J.-C. Latché, S. Minjeaud, and N. Therme. Conservativity and weak consistency of a class of staggered finite volume methods for the Euler equations. *Math. Comp.*, 90:1155–1177, 2021.
- [37] R. Herbin, J.-C. Latché, and T. T. Nguyen. Explicit staggered schemes for the compressible Euler equations. In *Applied mathematics in Savoie—AMIS 2012: Multiphase flow in industrial and environmental engineering*, volume 40 of *ESAIM Proc.*, pages 83–102. EDP Sci., 2013.
- [38] R. Herbin, J.-C. Latché, and T. T. Nguyen. Consistent segregated staggered schemes with explicit steps for the isentropic and full Euler equations. *ESAIM-Math. Model. Numer. Anal.*, 52(3):893–944, 2018.
- [39] R. Herbin, J.-C. Latché, and K. Saleh. Low Mach number limit of some staggered schemes for compressible barotropic flows. *Math. Comp.*, 90:1039–1087, 2021.
- [40] D. D. Houghton and A. Kasahara. Nonlinear shallow fluid flow over an isolated ridge. *NCAR Manuscript*, 259a, 1967.
- [41] S. Kaniel and J. Falcovitz. Approximation of the hydrodynamic equations by a transport process. In R. Rautman, editor, *Proceedings of IUTAM Symposium on Approximation Methods for Navier-Stokes Problems*, volume 771 of *Lecture Notes in Math*. Springer-Verlag, 1980.
- [42] W. Kheriji, R. Herbin, and J.-C. Latché. Pressure correction staggered schemes for barotropic one-phase and two-phase flows. *Computers & Fluids*, 88:524 – 542, 2013.

- [43] C. Klingenberg, G. Puppo, and M. Semplice. Arbitrary order finite volume well-balanced schemes for the Euler equations with gravity. *SIAM J. Sci. Comput.*, 41(2):A695–A721, 2019.
- [44] F. Lespagnol and G. Dakin. High order accurate schemes for Euler and Navier-Stokes equations on staggered Cartesian grids. *J. Comput. Phys.*, 410:109314, 2020.
- [45] R. LeVeque. Balancing source terms and flux gradients in high-resolution godunov methods: The quasi-steady wave-propagation algorithm. *J. Comput. Phys.*, 146(1):346–365, 1998.
- [46] R. J. LeVeque. *Finite volume methods for hyperbolic problems*. Cambridge Texts in Applied Mathematics. Cambridge University Press, Cambridge, 2002.
- [47] B. Perthame. Second order Boltzmann schemes for compressible Euler equations in one and two space dimension. *SIAM J. Numer. Anal.*, 29(1):1–19, 1992.
- [48] B. Perthame. *Kinetic formulation of conservation laws*. Oxford Lecture Series in Math. and its Appl. Oxford University Press, 2003.
- [49] G. Stelling and S. Duinmeijer. A staggered conservative scheme for every Froude number in rapidly varied shallow water flows. *Internat. J. Numer. Methods Fluids*, 43(12):1329–1354, 2003.
- [50] W. C. Thacker. Some exact solutions to the nonlinear shallow-water wave equations. *J. Fluid Mech.*, 107:499–508, 1981.
- [51] E. F. Toro. *Riemann solvers and numerical methods for fluid dynamics*. Springer-Verlag, Berlin, third edition, 2009.
- [52] D. R. van der Heul, C. Vuik, and P. Wesseling. A conservative pressure-correction method for flow at all speeds. *Computers & Fluids*, 32(8):1113–1132, 2003.
- [53] B. van Leer. Towards the ultimate conservative difference scheme. V. A second-order sequel to Godunov’s method. *J. Comput. Phys.*, 135(2):227–248, 1997. With an introduction by Ch. Hirsch, Commemoration of the 30th anniversary of J. Comput. Phys.
- [54] B. van’t Hof and A. E. P. Veldman. Mass, momentum and energy conserving (MaMEC) discretizations on general grids for the compressible Euler and shallow water equations. *J. Comput. Phys.*, 231(14):4723–4744, 2012.
- [55] J. VonNeumann and R. D. Richtmyer. A method for the numerical calculation of hydrodynamic shocks. *J. Appl. Phys.*, 21:232–237, 1950.
- [56] I. Wenneker, A. Segal, and P. Wesseling. A Mach-uniform unstructured staggered grid method. *Internat. J. Numer. Methods Fluids*, 40(9):1209–1235, 2002.
- [57] I. Wenneker, A. Segal, and P. Wesseling. Conservation properties of a new unstructured staggered scheme. *Computers & Fluids*, 32(1):139–147, 2003.
- [58] P. Wesseling. *Principles of computational fluid dynamics*, volume 29 of *Springer Series in Computational Mathematics*. Springer, 2001.
- [59] P. Woodward and P. Colella. The numerical simulation of two-dimensional fluid flow with strong shocks. *J. Comput. Phys.*, 54:115–173, 1984.